Modelling and simulation of traditional hydraulic heave compensation systems

Date:16-12-2016

R.V. Sanders - 1100475
University of Twente
Faculty of Engineering Technology
Supervisor: J.P. Schilder

Internship period:
Start: 12-09-2016
End: 16-12-2016

HYCOM B.V.
Antillen 43
7333 PE Apeldoorn
The Netherlands
Supervisors: A. Rondeel and W. Hoefakker.

Preface

The complexity of hydraulic heave compensation systems lies in the many different components, each with their own dynamics. In this report two methods of heave compensation systems are analysed, modelled and simulated. The methods distinguish in actuation, where one uses a hydraulic cylinder to adjust the cable length, the other does so by directly rotating a drum using a hydraulic motor. The goal of this research is to compare and quantify the performance and efficiency of the two systems.

Chapter 1 gives a description of a knuckle boom crane that is influenced by the wave-induced heave motion of a vessel, resulting in a translation of the load. A wave model is provided and the heave motion of the crane tip can then be determined through the kinematic equations of the crane. Also the cranes equation of motion is given and a suggestion for controlling its actuator coordinates in case the crane requires further development.

Chapter 2 offers dynamic models of some key features in the active heave system, such as the cable and drum model and the equation of motion of the load. The focus of this report lies on the dynamic behaviour of the hydraulic components described in Chapter 3. Two hydraulic systems are analysed, which differ in their actuation action. Starting with the translational system that consists of a hydraulic cylinder and a proportional valve. A linear model is given that offers the basis for the Simulink model. The rotational system is described in a similar fashion, it consists of a hydraulic motor and a proportional valve.

Accumulators are common components in hydraulic systems and are used to store energy by gas compression. More advanced translational systems improve efficiency by implementing a nitrogen accumulator that counters the inertia forces of the load. In these circumstances the gas model can rarely be described by the ideal gas equation. Therefore Chapter 4 offers a more complicated pressure-temperature model of a nitrogen accumulator.

In Chapter 5 a control strategy is given. The controller is tasked with regulating the fluid flow through the valve to either the hydraulic cylinder or motor to adjust the cable length and manipulate the position of the load. Velocity feedforward from the motion reference unit is used to counter the heave motion of the vessel. Feedback is used to compensate the remaining position error measured in the crane tip and stabilize the system. Also a control strategy is developed to counter the influence of the cable dynamics on the load.

The Simulink model is validated in Chapter 6 with respect to test results of a practical application of a rotational heave compensation system that HYCOM B.V. delivered for TMS. This gave insight on the correctness of the model and the abilities of the controller developed in Chapter 5. With that knowledge both translational and rotational compensation systems are simulated and compared in Chapter 7. That also offers insight on improvements regarding efficiencies for both actuation systems.

Contents

General definitions of symbols.

Symbol	Dimension	Definition
β	$\mathrm{Nm^{-2}}$	Bulk modulus
ζ	m	Vector of wave elevation.
η	$-$	Coefficient of efficiency
θ	rad	Angle
ρ	$\mathrm{kgm^{-3}}$	Density
ω	$\mathrm{rad \cdot s^{-1}}$	Frequency
a	$\mathrm{ms^{-2}}$	Acceleration
A	$\mathrm{m^2}$	Area
b	$\mathrm{Nsm^{-1}}$	Damping coefficient
b	m	Flow area coefficient
B	$\mathrm{Nsm^{-1}}$	Viscous friction coefficient
d	m	Diameter
D	$\mathrm{m^3rad^{-1}}$	Stroke volume
E	Pa	Modulus of elasticity
F	N	Force
h	$\mathrm{Wm^{-2}K^{-1}}$	Heat transfer coefficient
J	$\mathrm{kgm^2}$	Mass moment of inertia
k	$\mathrm{Nm^{-1}}$	Stiffness coefficient
L	m	Length
m	kg	Mass
M	$\mathrm{kg \cdot mol^{-1}}$	Molar mass
p	Pa	Pressure
P	W	Power
q	$\mathrm{m^3s^{-1}}$	Flowrate
R	$\mathrm{Pa \cdot m^3mol^{-1}K^{-1}}$	Gas constant
T	K	Temperature
T	Nm	Torque
U	J	Inertial energy
v	$\mathrm{m^3kg^{-1}}$	Specific volume
V	$\mathrm{m^3}$	Volume
w	m	Width
W	J	Work
x	m	Position

1 Crane model

1.1 Kinematics

A schematic knuckle boom crane is illustrated in figure 1. The crane consists of three rotational links; the rotary base is mounted on the vessel deck, the boom is connected to the base and the jib is the outermost link. The motion of the crane base is given by the motion reference unit (MRU) positioned at the crane base. A coordinate transformation is required to determine the displacement of the crane tip, the crane is assumed to be rigid.

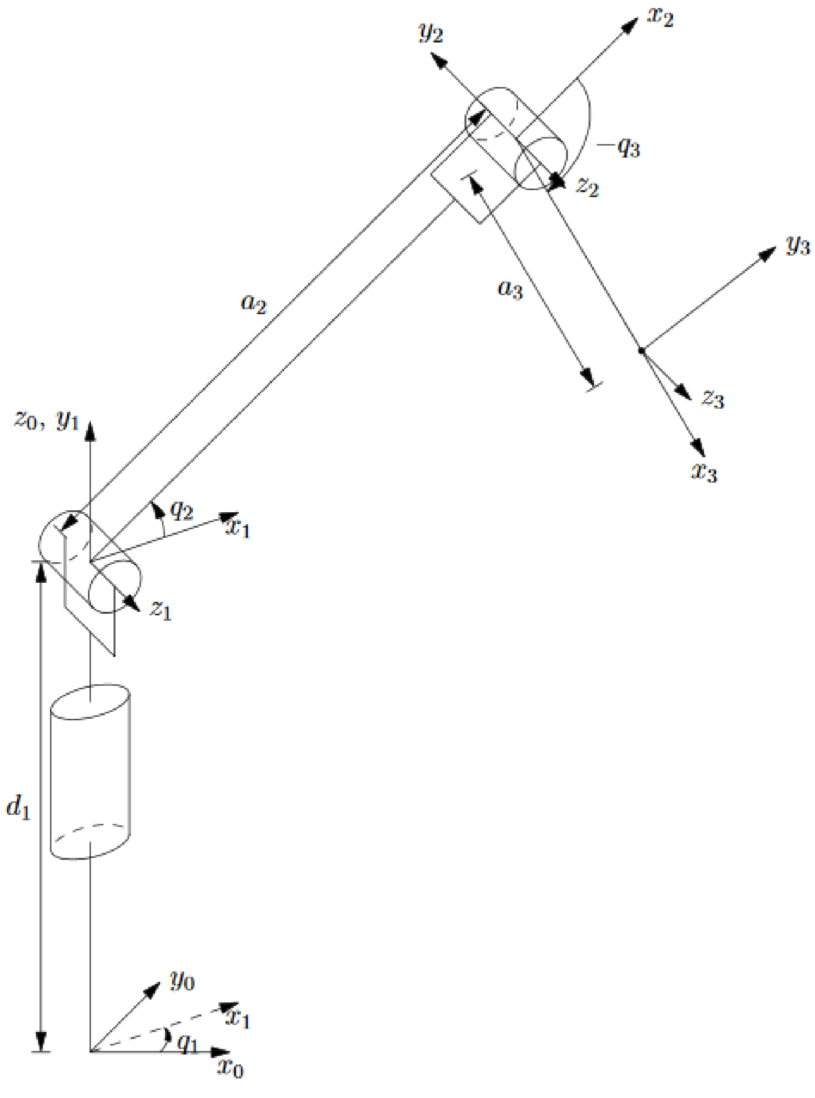

Figure 1 – Schematic knuckle boom crane [9].

Four coordinate frames O_i are shown in figure 1, with O_i denoting the origin of coordinate frame i. The parameters in figure 1 are defined as follows:

a_i is the distance from O_i to the intersection of the x_i and z_{i-1} axes.
d_i is the distance from O_{i-1} to the intersection of the x_i and z_{i-1} axes.
α_i is the angle between z_{i-1} and z_i about x_i.
q_i is the angle between x_{i-1} and x_i about z_{i-1}.

The definition of these parameters in accordance with figure 1 are given in table 1.

i	a_i	d_i	α_i	q_i
1	0	d_1	$\pi/2$	q_1
2	a_2	0	0	q_2
3	a_3	0	0	q_3

Table 1 - Parameters from figure 1.

The transformation matrices relate coordinate frame i to coordinate frame $i-1$ and consist of a rotation matrix $\boldsymbol{R}_{\boldsymbol{i}}^{i-1} \in \mathbb{R}^{3x3}$ and a position vector $\boldsymbol{p}_i^{i-1}$. The generic transformation matrix from frame i to frame $i-1$ is given in equation 1.1.

$$\boldsymbol{A}_i^{i-1} = \begin{bmatrix} \boldsymbol{R}_i^{i-1} & \boldsymbol{p}_i^{i-1} \\ 0^T & 1 \end{bmatrix} = \begin{bmatrix} c(q_i) & -s(q_i)c(\alpha_i) & s(q_i)s(\alpha_i) & a_i c(q_i) \\ s(q_i) & c(q_i)c(\alpha_i) & -c(q_i)s(\alpha_i) & a_i s(q_i) \\ 0 & s(\alpha_i) & c(\alpha_i) & d_i \\ 0 & 0 & 0 & 1 \end{bmatrix} \tag{1.1}$$

Where $c(\,)$ and $s(\,)$ stand for $\cos(\,)$ and $\sin(\,)$, respectively. The link specific transformation matrices are derived as:

$$\begin{aligned} \boldsymbol{A}_1^0 &= \begin{bmatrix} \boldsymbol{R}_1^0 & \boldsymbol{p}_1^0 \\ 0^T & 1 \end{bmatrix} = \begin{bmatrix} c(q_1) & 0 & s(q_1) & 0 \\ s(q_1) & 0 & -c(q_1) & 0 \\ 0 & 1 & 0 & d_1 \\ 0 & 0 & 0 & 1 \end{bmatrix} \\ \boldsymbol{A}_2^1 &= \begin{bmatrix} \boldsymbol{R}_2^1 & \boldsymbol{p}_2^1 \\ 0^T & 1 \end{bmatrix} = \begin{bmatrix} c(q_2) & -s(q_2) & 0 & a_2 c(q_2) \\ s(q_2) & c(q_2) & 0 & a_2 s(q_2) \\ 0 & 0 & 1 & 0 \\ 0 & 0 & 0 & 1 \end{bmatrix} \\ \boldsymbol{A}_3^2 &= \begin{bmatrix} \boldsymbol{R}_3^2 & \boldsymbol{p}_3^2 \\ 0^T & 1 \end{bmatrix} = \begin{bmatrix} c(q_3) & -s(q_3) & 0 & a_3 c(q_3) \\ s(q_3) & c(q_3) & 0 & a_3 s(q_3) \\ 0 & 0 & 1 & 0 \\ 0 & 0 & 0 & 1 \end{bmatrix} \end{aligned} \tag{1.2}$$

The transformation matrix for the end effector frame to the base frame is given by equation 1.3:

$$\boldsymbol{T}_n^0(\boldsymbol{q}) = \boldsymbol{A}_1^0(\boldsymbol{q})\boldsymbol{A}_2^1(\boldsymbol{q})\boldsymbol{A}_3^2(\boldsymbol{q}) \tag{1.3}$$

With $\boldsymbol{q} = [q_1\ q_2\ q_3]^T$, the resulting transformation matrix is

$$\boldsymbol{T}_n^0 = \begin{bmatrix} \boldsymbol{R}_3^0 & \boldsymbol{p}_3^0 \\ 0^T & 1 \end{bmatrix} \tag{1.4}$$

Where $\boldsymbol{R}_3^0$ is the orientation of coordinate frame 3 given in coordinate frame 0 and $\boldsymbol{p}_3^0$ is the position vector of the origin of coordinate frame 3 given in coordinate frame 0. For the base frame at rest, the position of the origin of the base frame is given as $\boldsymbol{p}_0^0(0) = (0,0,0)^T$, whereas the orientation of the base frame is given as

$$\boldsymbol{R}_0^0(0) = \begin{bmatrix} 1 & 0 & 0 \\ 0 & 1 & 0 \\ 0 & 0 & 1 \end{bmatrix} \tag{1.5}$$

This yields the transformation matrix for the base frame at rest.

$$\boldsymbol{T}_0^0(0) = \begin{bmatrix} \boldsymbol{R}_0^0 & \boldsymbol{p}_0^0 \\ 0^T & 1 \end{bmatrix} = \begin{bmatrix} 1 & 0 & 0 & 0 \\ 0 & 1 & 0 & 0 \\ 0 & 0 & 1 & 0 \\ 0 & 0 & 0 & 1 \end{bmatrix} \tag{1.6}$$

1.2 Differential kinematics

Differential kinematics relate the joint velocities and accelerations to the corresponding end effector (angular) velocities by using the geometric Jacobian $\boldsymbol{J}(\boldsymbol{q})$ in equation 1.7.

$$\boldsymbol{v} = \begin{bmatrix} \dot{\boldsymbol{p}} \\ \boldsymbol{\omega} \end{bmatrix} = \boldsymbol{J}(\boldsymbol{q})\dot{\boldsymbol{q}}, \quad \boldsymbol{J} = \begin{bmatrix} \boldsymbol{J}_p \\ \boldsymbol{J}_o \end{bmatrix} \tag{1.7}$$

$\dot{\boldsymbol{p}}$ is the crane tip linear velocity relative to the crane base and $\boldsymbol{\omega}$ is the angular velocity. The geometric Jacobian consists of two submatrices $\boldsymbol{J}_p$ and $\boldsymbol{J}_o$, that relate the joint velocities to the linear and angular velocities, respectively.

$$\begin{bmatrix} \boldsymbol{J}_p \\ \boldsymbol{J}_o \end{bmatrix} = \begin{bmatrix} J_{p_1} & J_{p_2} & J_{p_3} \\ J_{o_1} & J_{o_2} & J_{o_3} \end{bmatrix} \tag{1.8}$$

The expressions for the vectors depend on the behaviour of the corresponding joint, either prismatic or revolute. In the knuckle crane model all joint are revolute, they can be expressed as

$$\begin{bmatrix} J_{p_i} \\ J_{o_i} \end{bmatrix} = \begin{bmatrix} \boldsymbol{z}_{i-1} \times (\boldsymbol{p} - \boldsymbol{p}_{i-1}) \\ \boldsymbol{z}_{i-1} \end{bmatrix} \tag{1.9}$$

The vectors in equation ## are defined as follows:

$\boldsymbol{p}$ is the position vector in the transformation matrix $\boldsymbol{T}_n^0$.
$\boldsymbol{p}_{i-1}$ is the position vector in the transformation matrix $\boldsymbol{T}_{i-1}^0$.
$\boldsymbol{z}_{i-1}$ is the third column in the rotation matrix $\boldsymbol{R}_{i-1}^0$.

From which follows that:

$$\boldsymbol{p} = \begin{bmatrix} c(q_1)\left(a_3\big(c(q_2)c(q_3) - s(q_2)s(q_3)\big) + a_2 c(q_2)\right) \\ s(q_1)\left(a_3\big(c(q_2)c(q_3) - s(q_2)s(q_3)\big) + a_2 c(q_2)\right) \\ a_3\big(s(q_2)c(q_3) + c(q_2)s(q_3)\big) + a_2 s(q_2) + d_1 \end{bmatrix} \tag{1.10}$$

$$\boldsymbol{p}_0 = \begin{bmatrix} 0 \\ 0 \\ 0 \end{bmatrix}, \quad \boldsymbol{p}_1 = \begin{bmatrix} 0 \\ 0 \\ d_1 \end{bmatrix}, \quad \boldsymbol{p}_2 = \begin{bmatrix} a_2 c(q_1)c(q_2) \\ a_2 s(q_1)c(q_2) \\ a_2 s(q_2) + d_1 \end{bmatrix} \tag{1.11}$$

$$\boldsymbol{z}_0 = \begin{bmatrix} 0 \\ 0 \\ 1 \end{bmatrix}, \quad \boldsymbol{z}_1 = \begin{bmatrix} s(q_1) \\ -c(q_1) \\ 0 \end{bmatrix}, \quad \boldsymbol{z}_2 = \begin{bmatrix} s(q_1) \\ -c(q_1) \\ 0 \end{bmatrix} \tag{1.12}$$

The geometric Jacobian may now be expressed by the vectors in equations 1.10 - 1.12.

$$\boldsymbol{J} = \begin{bmatrix} \boldsymbol{z}_0 \times (\boldsymbol{p} - \boldsymbol{p}_0) & \boldsymbol{z}_1 \times (\boldsymbol{p} - \boldsymbol{p}_1) & \boldsymbol{z}_2 \times (\boldsymbol{p} - \boldsymbol{p}_2) \\ \boldsymbol{z}_0 & \boldsymbol{z}_1 & \boldsymbol{z}_2 \end{bmatrix} \tag{1.13}$$

The end effector acceleration can be derived by differentiating equation 1.7, resulting in equation 1.14:

$$\dot{\boldsymbol{v}} = \begin{bmatrix} \ddot{\boldsymbol{p}} \\ \dot{\boldsymbol{\omega}} \end{bmatrix} = \dot{\boldsymbol{J}}(\boldsymbol{q}, \dot{\boldsymbol{q}})\dot{\boldsymbol{q}} + \boldsymbol{J}(\boldsymbol{q})\ddot{\boldsymbol{q}} \tag{1.14}$$

$$\begin{bmatrix} \dot{j}_{p_i} \\ \dot{j}_{o_i} \end{bmatrix} = \begin{bmatrix} \dot{\boldsymbol{z}}_{i-1} \times (\boldsymbol{p} - \boldsymbol{p}_{i-1}) + \boldsymbol{z}_{i-1} \times (\dot{\boldsymbol{p}} - \dot{\boldsymbol{p}}_{i-1}) \\ \dot{\boldsymbol{z}}_{i-1} \end{bmatrix} \tag{1.15}$$

$$\dot{\boldsymbol{J}}(\boldsymbol{q}, \dot{\boldsymbol{q}}) = \begin{bmatrix} \dot{j}_{p_1} & \dot{j}_{p_2} & \dot{j}_{p_3} \\ \dot{j}_{o_1} & \dot{j}_{o_2} & \dot{j}_{o_3} \end{bmatrix} \tag{1.16}$$

1.3 Crane dynamics and control

The Lagrange formulation of the system is stated in equation 1.17.

$$\boldsymbol{B}(\boldsymbol{q})\ddot{\boldsymbol{q}} + \boldsymbol{C}(\boldsymbol{q}, \dot{\boldsymbol{q}})\dot{\boldsymbol{q}} + \boldsymbol{N}(\dot{\boldsymbol{q}}, \boldsymbol{q}) + \boldsymbol{G}(\boldsymbol{q}) = \boldsymbol{\tau} - \boldsymbol{J}^T(\boldsymbol{q})\boldsymbol{f} \tag{1.17}$$

With $\boldsymbol{B}(\boldsymbol{q})$ representing the inertia matrix, $\boldsymbol{C}(\boldsymbol{q}, \dot{\boldsymbol{q}})$ and $\boldsymbol{N}(\dot{\boldsymbol{q}}, \boldsymbol{q})$ the matrix of Coriolis and centripetal forces and $\boldsymbol{G}(\boldsymbol{q})$ the geometric dependent forces, like gravity. The first term on the right hand side are the generalized torques $\boldsymbol{\tau} = [\tau_1\ \tau_2\ \tau_3]^T$ acting in the respective joints. In practice the torques τ_2 and τ_3 are generated with hydraulic cylinders. The second term on the right hand side is the end effector force through the geometric Jacobian $\boldsymbol{J}(\boldsymbol{q})$ defined in paragraph 1.2. $\boldsymbol{f}$ will be equal in magnitude but opposite in direction from the force exerted by the hoisting cable.

This equation of motion describes a fully actuated manipulator with nonlinear MiMo (multi-input multi-output) dynamics in actuator coordinates. In controlling such a manipulator it is key to decouple the system so that each degree of freedom can be actuated independently. It is suggested to use a method called *Computed Torque Control*, abbreviated as CTC. This controller would be of the form:

$$\boldsymbol{\tau} = \boldsymbol{B}(\boldsymbol{q})\boldsymbol{C}_f(\boldsymbol{r}, \dot{\boldsymbol{r}}, \ddot{\boldsymbol{r}}, \boldsymbol{q}, \dot{\boldsymbol{q}}) + \boldsymbol{C}(\boldsymbol{q}, \dot{\boldsymbol{q}})\dot{\boldsymbol{q}} + \boldsymbol{N}(\dot{\boldsymbol{q}}, \boldsymbol{q}) + \boldsymbol{G}(\boldsymbol{q}) + \boldsymbol{J}^T(\boldsymbol{q})\boldsymbol{f} \tag{1.18}$$

With $\boldsymbol{C}_f$ being some feedback controller discussed later. Substitution in the equation of motion yields

$$\boldsymbol{B}(\boldsymbol{q})\ddot{\boldsymbol{q}} = \boldsymbol{B}(\boldsymbol{q})\boldsymbol{C}_f(\boldsymbol{r}, \dot{\boldsymbol{r}}, \ddot{\boldsymbol{r}}, \boldsymbol{q}, \dot{\boldsymbol{q}}) \tag{1.19}$$

The inertia matrix of a well-defined mechanical system, expressed in a set of degrees of freedom, is non-singular and thus its inverse exist. This makes it possible to control the acceleration of each degree of freedom independently with controller $\boldsymbol{C}_f$.

$$\ddot{\boldsymbol{q}} = \boldsymbol{C}_f(\boldsymbol{r}, \dot{\boldsymbol{r}}, \ddot{\boldsymbol{r}}, \boldsymbol{q}, \dot{\boldsymbol{q}}) \tag{1.20}$$

This approach does require the measurement of position and velocity of each degree of freedom. Two essential elements in the controller are; feedback compensation for all position and velocity dependent dynamic forces and linearization and decoupling of the controller by the inertia matrix.

A standard controller $\boldsymbol{C}_f$ would be in the form:

$$\boldsymbol{C}_f(\boldsymbol{r}, \dot{\boldsymbol{r}}, \ddot{\boldsymbol{r}}, \boldsymbol{q}, \dot{\boldsymbol{q}}) = \ddot{\boldsymbol{r}} + k_p(\boldsymbol{r} - \boldsymbol{q}) + k_d(\dot{\boldsymbol{r}} - \dot{\boldsymbol{q}}) \tag{1.21}$$

Where the first term is acceleration feedforward of the reference signal and the other terms describe a basic PD controller. The feedforward applies forces to make the system trace reference $\boldsymbol{r}$, whereas the PD controller stabilises the system by counteracting unknown disturbances. Feedback is required since a system with CTC control is only marginally stable.

1.4 Vessel motion

The vessel motion can be implemented through transformation of the base frame.

$$\boldsymbol{T}_0^h = \begin{bmatrix} \boldsymbol{R}_0^h & \boldsymbol{p}_0^h \\ 0^T & 1 \end{bmatrix} \tag{1.22}$$

The position of the origin of the base frame depends on the position of the vessel.

$$\boldsymbol{p}_0^h = (x, y, z)^T \tag{1.23}$$

The orientation of the base frame in time depends on the Euler angles that denote the roll, pitch and yaw angle of the vessel, respectively. The rotation matrix of the base frame is therefore given by:

$$\boldsymbol{R}_0^h = \begin{bmatrix} c(\psi)c(\theta) & -s(\psi)c(\phi) + c(\psi)s(\theta)s(\phi) & s(\psi)s(\phi) + c(\psi)c(\phi)s(\theta) \\ s(\psi)c(\theta) & c(\psi)c(\phi) + s(\phi)s(\theta)s(\psi) & -c(\psi)s(\phi) + s(\theta)s(\psi)c(\phi) \\ -s(\theta) & c(\theta)s(\phi) & c(\theta)c(\phi) \end{bmatrix} \tag{1.24}$$

The transformation matrix for the base frame is given by:

$$\boldsymbol{T}_0^h = \begin{bmatrix} c(\psi)c(\theta) & -s(\psi)c(\phi) + c(\psi)s(\theta)s(\phi) & s(\psi)s(\phi) + c(\psi)c(\phi)s(\theta) & x \\ s(\psi)c(\theta) & c(\psi)c(\phi) + s(\phi)s(\theta)s(\psi) & -c(\psi)s(\phi) + s(\theta)s(\psi)c(\phi) & y \\ -s(\theta) & c(\theta)s(\phi) & c(\theta)c(\phi) & z \\ 0 & 0 & 0 & 1 \end{bmatrix} \tag{1.25}$$

When considering the heave motion in time, the time derivatives of position and orientation are required. For the position the time derivate is $\dot{\boldsymbol{p}}_0^h = (\dot{x}, \dot{y}, \dot{z})$. The time derivative of $\boldsymbol{R}_0^h(\phi, \theta, \psi)$ is per definition given by:

$$\dot{\boldsymbol{R}}_0^h\left(\phi, \dot{\phi}, \theta, \dot{\theta}, \psi, \dot{\psi}\right) = \boldsymbol{S}_0^h\left(\dot{\phi}, \dot{\theta}, \dot{\psi}\right)\boldsymbol{R}_0^h(\phi, \theta, \psi) \tag{1.26}$$

With $\boldsymbol{S}_0\left(\dot{\phi}, \dot{\theta}, \dot{\psi}\right)$ the skew-symmetric matrix

$$\boldsymbol{S}_0^h\left(\dot{\phi}, \dot{\theta}, \dot{\psi}\right) = \begin{bmatrix} 0 & -\dot{\psi} & \dot{\theta} \\ \dot{\psi} & 0 & -\dot{\phi} \\ -\dot{\theta} & \dot{\phi} & 0 \end{bmatrix} \tag{1.27}$$

These transformation matrices can be reduced by considering only the heave motion of the vessel, which yields the condition: $x = y = \psi = 0$, since these only cause displacement in the xy −plane.

$$\boldsymbol{T}_0^h(\phi, \theta, z) = \begin{bmatrix} c(\theta) & s(\theta)s(\phi) & c(\phi)s(\theta) & 0 \\ 0 & c(\phi) & -s(\phi) & 0 \\ -s(\theta) & c(\theta)s(\phi) & c(\theta)c(\phi) & z \\ 0 & 0 & 0 & 1 \end{bmatrix} \tag{1.28}$$

In general, when assuming a rigid and static crane with the defined configuration from table 1, the position of the boom tip under heave motion of the vessel can be derived with:

$$\boldsymbol{p}_3^h = \boldsymbol{p}_0^h + \boldsymbol{R}_0^h\boldsymbol{p}_3^0 \tag{1.29}$$

$$\dot{\boldsymbol{p}}_3^h = \dot{\boldsymbol{p}}_0^h + \dot{\boldsymbol{R}}_0^h\boldsymbol{p}_3^0 + \boldsymbol{R}_0^h\dot{\boldsymbol{p}}_3^0 = \dot{\boldsymbol{p}}_0^h + \boldsymbol{S}_0^h\boldsymbol{R}_0^h\boldsymbol{p}_3^0 + \boldsymbol{R}_0^h\dot{\boldsymbol{p}}_3^0 \tag{1.30}$$

1.5 Wave model

The wave model is provided by the MATLAB toolbox Marine Systems Simulator (MSS) [2]. The toolbox computes the wave elevation and speed in time at any given *x* and *y* position in the sea chart from figure 2:

$$\zeta(x,y,t) = \sum_{i=1}^{n} \zeta_a(i)\cos[\omega(i)t + \varphi(i) - k(i)(x\,cos(\psi(i)) + y\,sin(\psi(i)))] \tag{1.31}$$

Where:

ζ_a = Vector of harmonic wave amplitudes [m].
ω = Vector of harmonic wave frequencies [rad/s].
φ = Vector of harmonic wave phases (random) [rad].
k = Vector of harmonic wave numbers [1/m].
ψ = Vector of harmonic wave directions [rad].

This wave model is using superposition of different sine frequencies and amplitudes to generate a wave pattern. Figure 2 shows an example of the sea state realization using the MSS toolbox [2], the vessel can be located at any given position $[x, y, z]$ in figure 2.

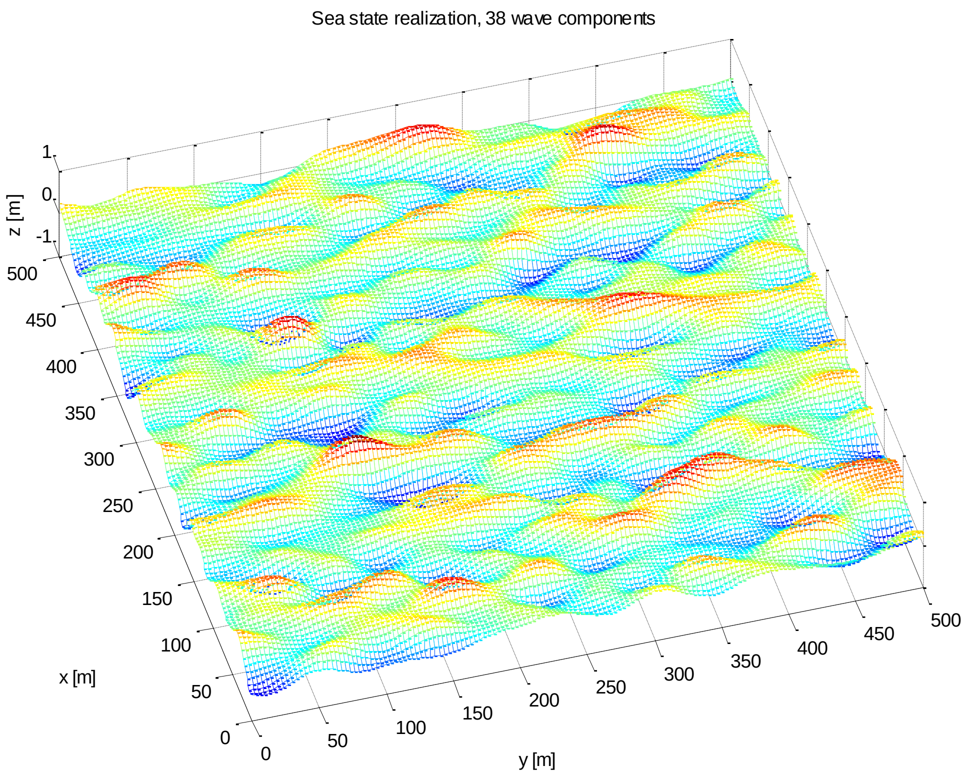

Figure 2 - Sea state realization using 38 wave components, created with the MSS MATLAB toolbox [2].

The wave model is directly used as motion reference unit (MRU) output, neglecting effects of the vessel on the heave motion. This is motivated as requiring the active heave compensation (AHC) system to be used on any given ship and not a particular one.

2 Payload and hoisting mechanism

Figure 3 shows a schematic model for raising and lowering a load attached to a cable by means of a winch. The winch is placed at the base of the knuckle boom crane that is described in Chapter 1. The cable is guided over the crane by means of guiding sheaves. The friction forces in these sheaves are not taken into account in the extend of this report. The models for the remaining parts are derived in this chapter.

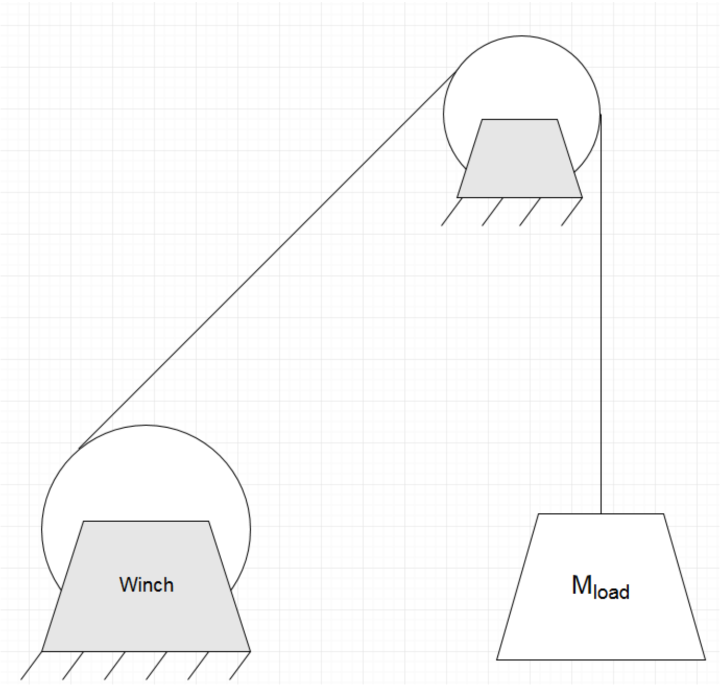

Figure 3 – Simplified model of winch and load.

2.1 Cable model

The cable is modelled as a stiff spring with stiffness coefficient k_c.

$$k_c = \frac{E\ A_c}{L_c} \tag{2.1}$$

E is the modulus of elasticity. A_c is the cross-sectional area of the cable, which is assumed constant throughout the simulation. The spring stiffness is inversely proportional to the cable length L_c.

Due to elongation and especially because of bending, energy losses occur in the cable. These losses originate from the friction between different strands in the cable. The damping coefficient is approximated as a ratio between the cable stiffness and mass, see equation 2.2.

$$b_c = 2\zeta\sqrt{k_c m_c} \tag{2.2}$$

Dimensionless damping coefficient ζ has a value of 0.1. The mass of the cable is defined by m_c and is proportional to the cable length L_c. Half of this mass is placed at the bottom of the cable, attached to the load. The other half is placed at the top of the cable in the crane tip.

$$m_c = \rho A_c L_c \tag{2.3}$$

Traditionally steel cables are used for offshore operations As greater depths are reached, the weight of the cable becomes more and more important, such that these days a trend towards high modulus polymers is set.

The force F_c in the cable is proportional to the cable elongation δL_c, using Hooke's law.

$$F_c = k_c \delta L_c \tag{2.4}$$

The natural frequency of a cable with load M_l is approximated with:

$$\omega_c = \sqrt{\frac{k_c}{M_l + m_c(L)}} \tag{2.5}$$

The natural frequency of the cable is proportional to a factor $\sqrt{\frac{1}{L}}$. In order to verify the Simulink model, table 2 compares frequencies derived analytically with frequencies extracted from the Simulink model.

Cable length (m)	Frequency (Hz)	
	Hand calculation	Simulink
1	5.3216	5.4601
500	0.2359	0.2422
1000	0.1653	0.1694
2000	0.1149	0.1179
3000	0.0923	0.0947

Table 2 - Estimated natural frequencies of the cable with load.

2.2 Load model

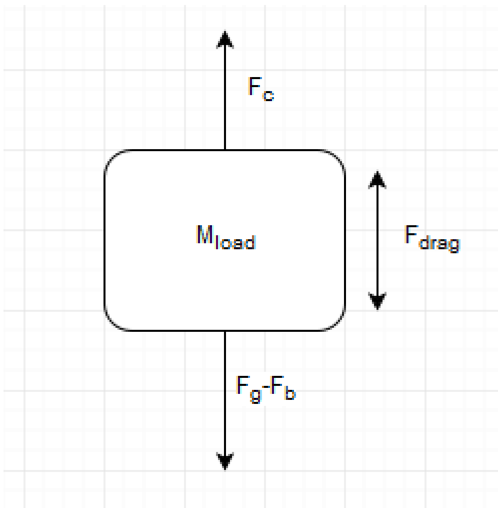

Figure 4

The motion of the load is modelled according to Newton's second law.

$$M_{tot}\,\ddot{x}_l + b_l(\dot{x}_l)\dot{x}_l + F_g - F_b = F_c \tag{2.6}$$

The mass M_{tot} contains the mass of the load M_l, the added mass from displaced water m_a and a percentage of the mass of the cable m_c, depending on the cable mass distribution. For simplicity half the cable mass is placed at the bottom of the cable, attached to the load. The other half is placed at the top of the cable in the crane tip ($n = 2$).

$$M_{tot} = M_l + m_a + \frac{1}{n} m_c \tag{2.7}$$

The damping factor $b_l(\dot{x}_l)$ represents viscous damping due to vortex shedding [3].

$$b_l(\dot{x}_l)\dot{x}_l = \frac{1}{2}\rho C_d A_f |\dot{x}_l| \dot{x}_l \tag{2.8}$$

2.3 Winch model

The drum and most important drum dimensions are shown in figure 5.

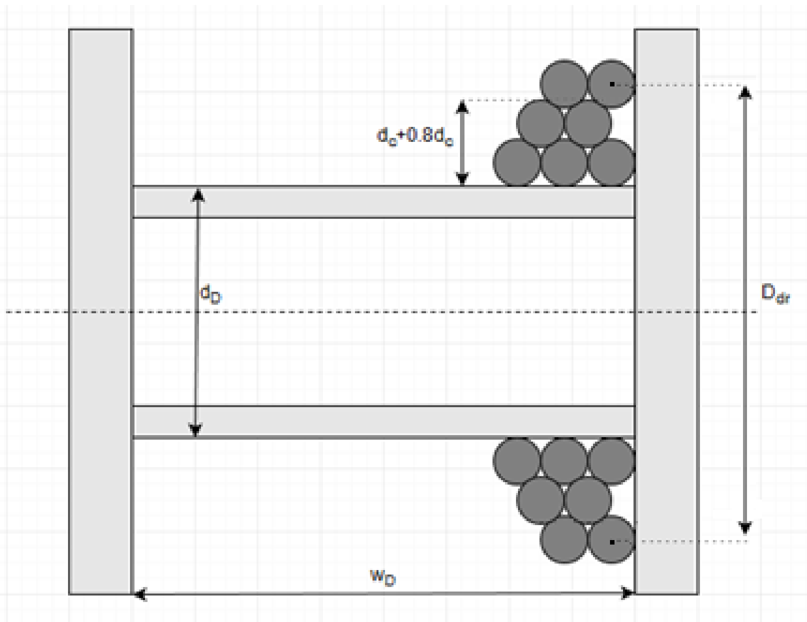

Figure 5 – Drum and cable dimensions.

The effective drum diameter is derived from figure 5 and depends on the number of layers of cable on the drum, see equation 2.9.

$$D_{dr} = d_D + d_c + 2(n-1) \cdot 0.8 d_c \tag{2.9}$$

The parameter n denotes the number of layers, d_c is the diameter of the cable and d_D is the base diameter of the drum. Besides the effective drum diameter, it is beneficial to estimate the cable length per layer. This is determined by using the ratio between drum width and cable diameter.

$$L_{cd} = \pi D_{dr} \frac{w_D}{d_c} \tag{2.10}$$

The inertia of a full layer is defined in equation 2.11.

$$J_{layer} = \rho A_c L_{cd} \cdot \left(\frac{D_{dr}}{2}\right)^2 \tag{2.11}$$

3 Active heave compensation

Active heave compensation is achieved by raising and lowering the load attached to a cable in counter phase to the translation of the crane tip that is caused by the wave-induced heave motion of a vessel. This is performed either by translation of a hydraulic cylinder as in figure 6 or by rotating the drum with a hydraulic motor. An advantage of the translational model is the fact that one ignores the mass of the spare cable that is still on the drum, whereas a rotational model has to rotate that entire inertia at all times. A drawback is that the cylinder requires multiple guiding sheaves that significantly decrease the lifetime of the cable.

The performance of the cylinder and motor are both limited by their reaction speed and the cylinder is also limited by its stroke. This often results in over-dimensioned systems with poor efficiencies. The translational systems often improve efficiencies by means of a nitrogen accumulator unit. The pressure from the accumulator can relief the system of inertia forces, such that the active cylinder can reduce substantially in size, requiring less fluid flow. More advanced rotational actuation systems acquire a better efficiency by using motors with a variable stroke volume that can adjust the stroke volume to the given load case.

Dynamic models for both actuation systems are derived in this chapter. The resulting Simulink models are verified with respect to their corresponding transfer functions. The working principle of both systems is explained by means of an example.

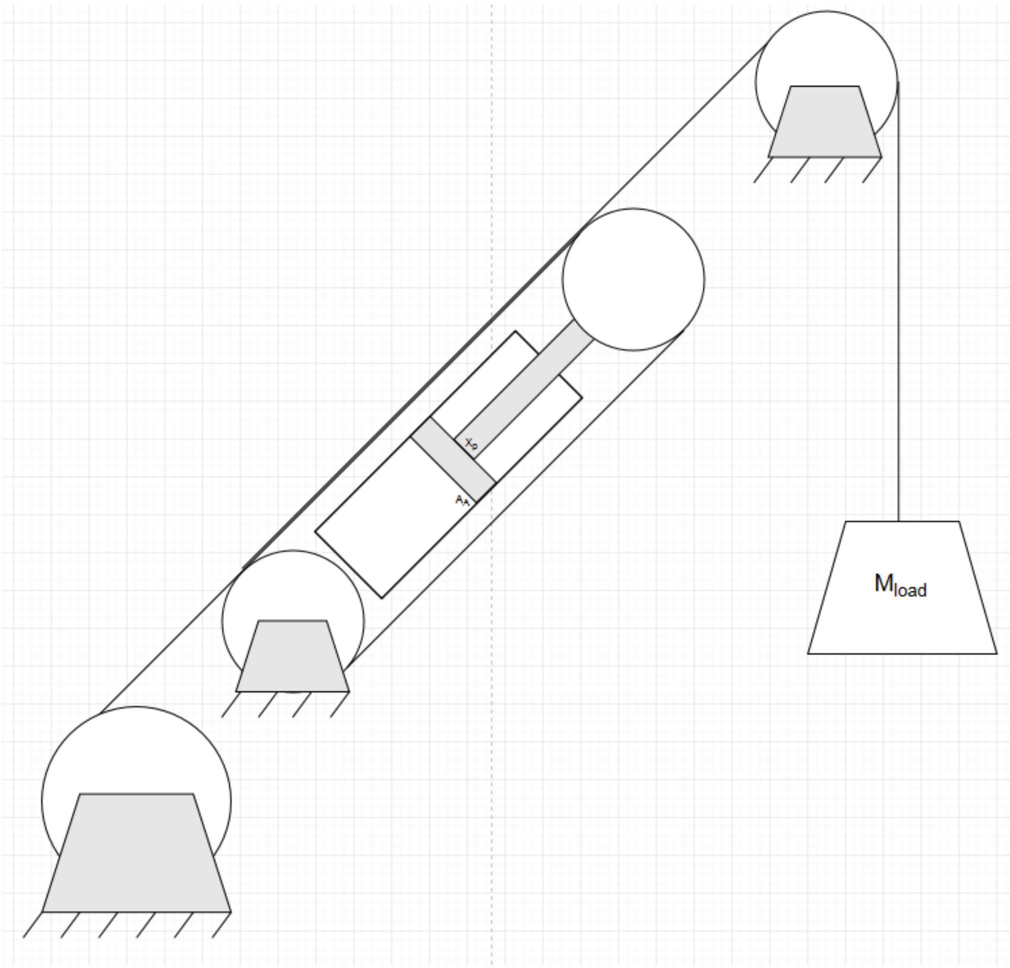

Figure 6 – Schematic view of heave compensation systems.

3.1 Translational system design

The two main components in the active heave compensation system are the servo valve and the hydraulic cylinder, see figure 7. The servo valve controls the flow in and out of the cylinder, while the hydraulic cylinder positions itself to compensate the load for the heave motion of the vessel.

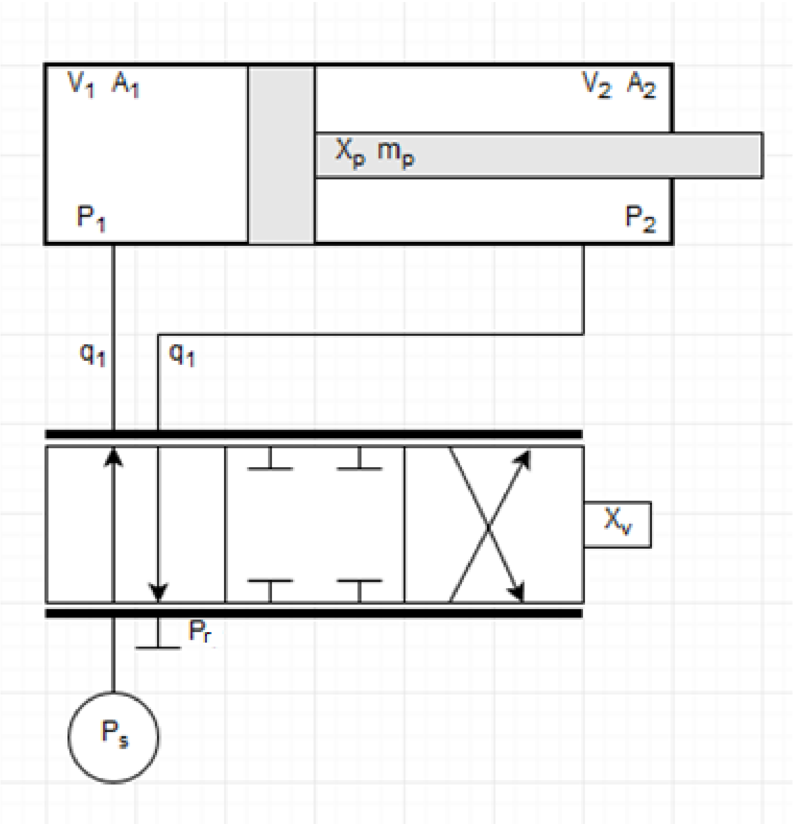

Figure 7 – Schematic double-acting cylinder controlled by a four-way valve.

It is common practice to dimension the system based upon a suitable supply pressure p_s [5]. This supply pressure can be used to determine the allowable load pressure p_L by calculating the maximum power delivered through the valve.

$$P = q_L p_L \tag{3.1}$$

Here q_L represents the flow rate through the valve, which needs to be large enough to retain precise control. The load flow of a matched and symmetric valve with a symmetric load can be expressed by:

$$q_L = C_d b x_v \sqrt{\frac{1}{\rho}(p_s - sgn(x_v)p_L)} \tag{3.2}$$

C_d = discharge coefficient (-)
b = flow area coefficient (m)
x_v = spool position (m)
p_s = supply pressure (Pa)
p_L = load pressure (Pa)

The assumption of a symmetric load implies that the flow in and out of the cylinder is equal, meaning that the compressibility of the fluid is not accounted for. This assumption yields simple transfer functions with sufficiently small errors to be used for static dimensioning.

Substituting 3.2 in equation 3.1 gives:

$$P = q_L p_L = C_d b x_v \sqrt{\frac{1}{\rho}(p_s - sgn(x_v)p_L)} \cdot p_L \tag{3.3}$$

The load pressure which yields the maximum power is found with:

$$\frac{dP}{dp_L} = C_d b x_v \sqrt{\frac{1}{\rho}} \left[\sqrt{(p_s - sgn(x_v)p_L)} - \frac{p_L}{2} \frac{1}{\sqrt{(p_s - sgn(x_v)p_L)}} \right] = 0 \tag{3.4}$$

From equation 3.4 we can derive that $|p_L| < \frac{2}{3} p_s$ [5]. This load pressure p_L can be used to determine the required area of the cylinder piston in equation 3.5. The effective piston area depends on the maximum force F_{max}, the load pressure p_L and the coefficient of efficiency η_m.

$$A_p = \frac{F_{max}}{p_L \cdot \eta_m} \tag{3.5}$$

Having determined the piston area and load pressure, the system is able to deliver the required force. However, to obtain a satisfactory heave compensation system the system must have a sufficient reaction time. The maximum piston velocity must be large enough to compensate for the vessels motion, this requires a volume flow Q_{max} given in equation 3.6.

$$Q_{max} = \frac{A_p v_{p_{max}}}{\eta_v} \tag{3.6}$$

For a given spool position the fluid passes through a four way valve twice. The non-distributed supply pressure is divided equally over the two passes, as a result of the assumptions made in equation 3.2. Considering the condition for p_L, the pressure drop for each pass then becomes $\Delta p = \frac{(p_s - p_L)}{2} = \frac{1}{4} p_L$. The flow through the valve is described by:

$$Q = C_d A_v \sqrt{\frac{2\Delta p}{\rho}} = C_d A_v \sqrt{\frac{p_L}{2\rho}} \tag{3.7}$$

The flow area required to deliver a flow rate of $Q = Q_{max}$ is determined with equation 3.8.

$$A_v = \frac{Q_{max}}{C_d \sqrt{\frac{p_L}{2\rho}}} \tag{3.8}$$

The flow area coefficient b depends on the maximum piston displacement inside the valve x_v.

$$b = \frac{A_v}{x_v} \tag{3.9}$$

3.2 Linear model

The mass balances for the two chambers of the cylinder and the equation of motion for the piston yields the following dynamic model of the active system [7]

$$\frac{V_{10} + A_1 x_p}{\beta}\dot{p}_1 = -C_{im}(p_1 - p_2) - C_{em}p_1 - A_1\dot{x}_p + q_1 \tag{3.10}$$

$$\frac{V_{20} - A_2 x_p}{\beta}\dot{p}_2 = -C_{im}(p_2 - p_1) - C_{em}p_2 + A_2\dot{x}_p + q_2 \tag{3.11}$$

$$m_t\ddot{x}_p = -B_p\dot{x}_p + A_1p_1 - A_2p_2 - F_L \tag{3.12}$$

In this balance q_1 and q_2 are the flows in and out of the two chambers. C_{im} and C_{em} represent the internal leakage and the external leakage respectively. Internal leakage is leakage from one chamber to another, whereas external leakage is leakage to either the drain or tank. β represents the effective bulk modulus of the fluid. m_t is the mass of the piston and the sheave combined. B_p is the viscous friction coefficient and F_L is the load force.

Assuming the cylinder is matched and symmetric and the load is assumed symmetric, equations 3.10 and 3.11 can be combined to yield 3.13.

$$\frac{V_t}{\beta}\dot{p}_L = -C_{tp}p_L - A_p\dot{x}_p + q_L \tag{3.13}$$

$$\begin{aligned} V_t &= \frac{1}{2}\left(V_{10} + V_{20} + \mathrm{A_p x_{p_0}}\right) \\ p_L &= p_1 - p_2 \\ C_{tp} &= C_{im} + \frac{1}{2}C_{em} \\ q_L &= \frac{1}{2}(q_1 + q_2) \end{aligned}$$

A matched and symmetric cylinder means that the upper and lower piston areas are equal, which is obviously not true due to the piston rod area. However, for sake of simplicity we can take the a theoretical value $A_p = \frac{A_1 + A_2}{2}$ during the controller design phase (note that during the simulations the cylinder is not assumed symmetric). The linear flow equations is given by 3.14.

$$q_L = K_q x_v - K_c p_L \tag{3.14}$$

Where $K_q = \frac{\partial q_L}{\partial x_v}$ and $K_c = -\frac{\partial q_L}{\partial p_L}$ are the coefficients of linearization. For an ideal flow-control valve the theoretical pressure-flow coefficient K_c would be zero, however this is not the case in practice. An ideal valve has perfect geometry so that leakage flows are zero. A practical valve has radial clearance and perhaps some under- or overlap of about $5 - 25\mu m$ [7].

The total linear model is expressed as:

$$\frac{V_t}{\beta}\dot{p}_L = -C_{tp}p_L - A_p\dot{x}_p + q_L \tag{3.15}$$

$$m_t\ddot{x}_p = -B_p\dot{x}_p + A_p p_L - F_L \tag{3.16}$$

$$q_L = K_q x_v - K_c p_L \tag{3.17}$$

Assuming no leakage and for $B_p \neq 0$ the Laplace transform of the model yields the transfer function for the piston position control $\frac{x_p(s)}{x_v(s)}$ in equation 3.18 [5]. Note that in case of position control the force input is assumed constant $\left(F_L = F_{L_0}\right)$.

$$\frac{x_p(s)}{x_v(s)} = \frac{\frac{K_q}{A_p} - \frac{K_c}{A_p^2}\left(1 - \frac{s}{\omega_t}\right) F_L}{s\left(1 + 2\zeta_h \frac{s}{\omega_h} + \frac{s^2}{\omega_h^2}\right)} \tag{3.18}$$

With parameters:

$$\omega_h = \sqrt{\frac{\beta A_p^2}{V_t m_t}}, \qquad \zeta_h = \frac{B_p}{A_p}\sqrt{\frac{V_t}{\beta m_t}}, \qquad \omega_t = \frac{\beta K_c}{V_t} \tag{3.19}$$

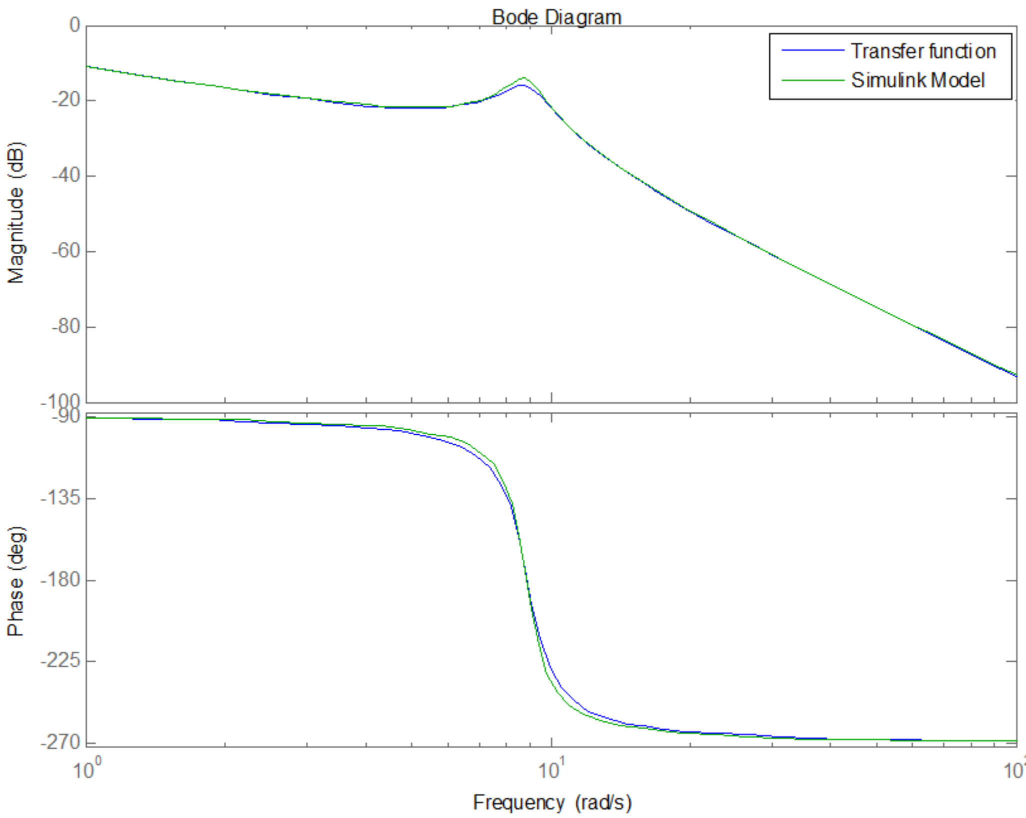

Figure 8 – Bode plot comparison between transfer function and Simulink cylinder model.

Figure 8 shows the bode plot of the analytical model and the Simulink model, it can be concluded that the Simulink model offers a good approximation of the theory. Both plots show the resonance frequency of the piston at approximately $\omega_h \approx 88\ rad/s$ obtained at position $x_{p_0} = \frac{1}{2} \cdot x_{p_{max}}$, which is the lowest natural frequency as piston stiffness increases when the piston comes closer to its end positions. Viscous damping coefficient is considered low at $\zeta_h = 0.1$.

3.3 Example translational system

Figures 9 and 10 show some simulation results of the translational heave compensation system. Figure 9 shows the flow behaviour through the proportional four-way valve. When the vessel rises the cable length needs to be extended, so the piston moves down. This corresponds to a positive flow q_2 and a negative flow q_1 and vice versa. Notable about the flows is the fact that q_2 is substantially smaller than q_1, because some volume is occupied by the piston rod. Figure 10 shows the pressures in cylinder chamber 1 and 2, respectively

The load pressure over the cylinder is defined by $P_L = P_1 - P_2$. At time $t = 0$ the initial load pressure is about $160\ bar$, which counters the static forces of the load. As the simulation continues the heave motion of the vessel will introduce a dynamic force in the cable that results in a displacement of the load. The four-way valve will regulate the flow in and out of the cylinder to move the piston in counter phase with the heave motion. In the ideal situation the piston will exactly trace the heave motion to nullify the dynamic force in the cable and keeping the load at its prescribed location.

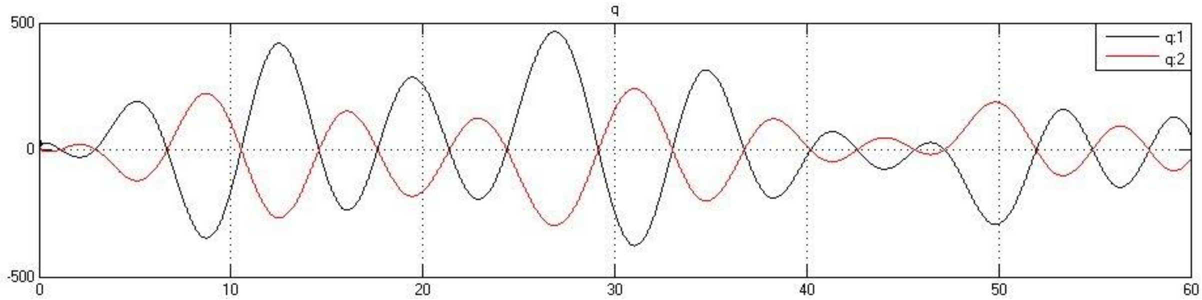

Figure 9 – Fluid flow q_1 and q_2 [L/min] from four-way valve to cylinder chamber 1 and 2, respectively, vs time [s].

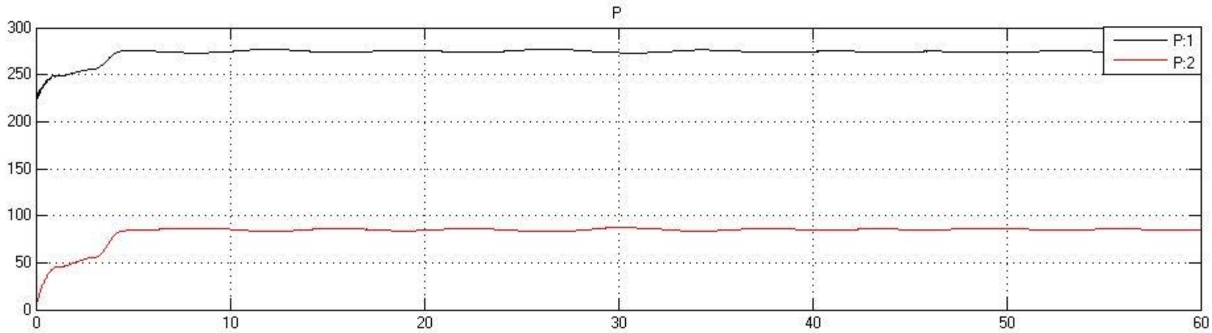

Figure 10 – Pressures [Bar] in cylinder chamber 1 and 2, respectively, versus time [s].

3.4 Rotational system design

In this composition the hydraulic cylinder from paragraph 3.1 is replaced with a hydraulic motor that is still controlled with the four way valve, see figure 11. All the nonlinearities existing in a valve controlled cylinder system still exist here. However, an additional problem is that the displacement volume in the motor is no longer constant but varies in a discontinuous fashion with the shaft rotation. By using a motor with a high number of pistons the amplitude of the kinematic displacement variation will be small enough to be neglected in dynamic calculations [7].

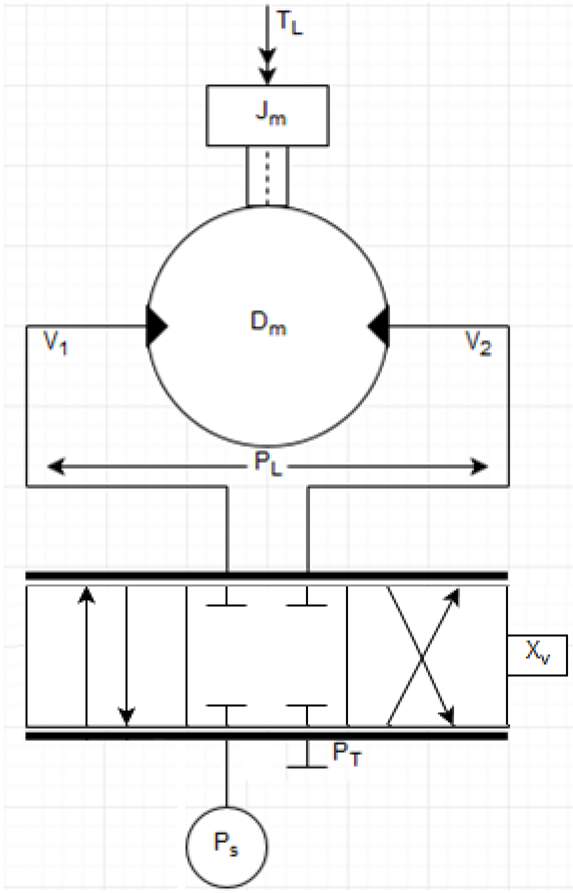

Figure 11 – Schematic hydraulic motor controlled by a four-way valve.

Assuming volume $V_1 = V_2$. The required motor stroke volume to counter a given load torque T_L depends on the pressure drop over the motor and the motor efficiency, see equation 3.23 [3].

$$D_m = \frac{T_{max}}{p_L \cdot \eta_m} \tag{3.23}$$

The required flow volume Q_m is depends on the motor stroke volume D_m and the required angular shaft speed ω_m and the volumetric efficiency, as in equation 3.24.

$$Q_m = \frac{D_m \cdot \omega_m}{\eta_v} \tag{3.24}$$

The linear model of the rotational system is similar to that of the translational system from equations 3.15 - 3.17. The main difference is working with volumes and torques instead of areas and forces.

$$\frac{V_m}{\beta}\dot{p}_L = -C_{tp}p_L - D_m\dot{\theta}_m + q_L \tag{3.25}$$

$$J_m\ddot{\theta}_m = -B_m\dot{\theta}_m + D_m p_L - T_L \tag{3.26}$$

$$q_L = K_q x_v - K_c p_L \tag{3.27}$$

In the same fashion as for the translational system leakage is neglected. This is a valid assumption for the translational system, but not realistic in case of a hydraulic motor. However, for only validating the Simulink model the assumption is allowed. For $B_m \neq 0$ the Laplace transform of the model yields the transfer function for position control $\frac{\theta_m(s)}{x_v(s)}$ in equation 3.18. Note that in case of position control the torque input is assumed constant $\left(T_L = T_{L_0}\right)$.

$$\frac{\theta_m(s)}{x_v(s)} = \frac{\frac{K_q}{D_m} - \frac{K_c}{D_m^2}\left(1 - \frac{s}{\omega_t}\right)T_L}{s\left(1 + 2\zeta_h\frac{s}{\omega_h} + \frac{s^2}{\omega_h^2}\right)} \tag{3.28}$$

With parameters:

$$\omega_h = \sqrt{\frac{\beta D_m^2}{V_m J_m}}, \qquad \zeta_h = \frac{B_m}{D_m}\sqrt{\frac{V_m}{\beta J_m}}, \qquad \omega_t = \frac{\beta K_c}{V_m} \tag{3.29}$$

Figure 12 validates the Simulink model of the hydraulic motor with respect to the transfer function from equation 3.28.

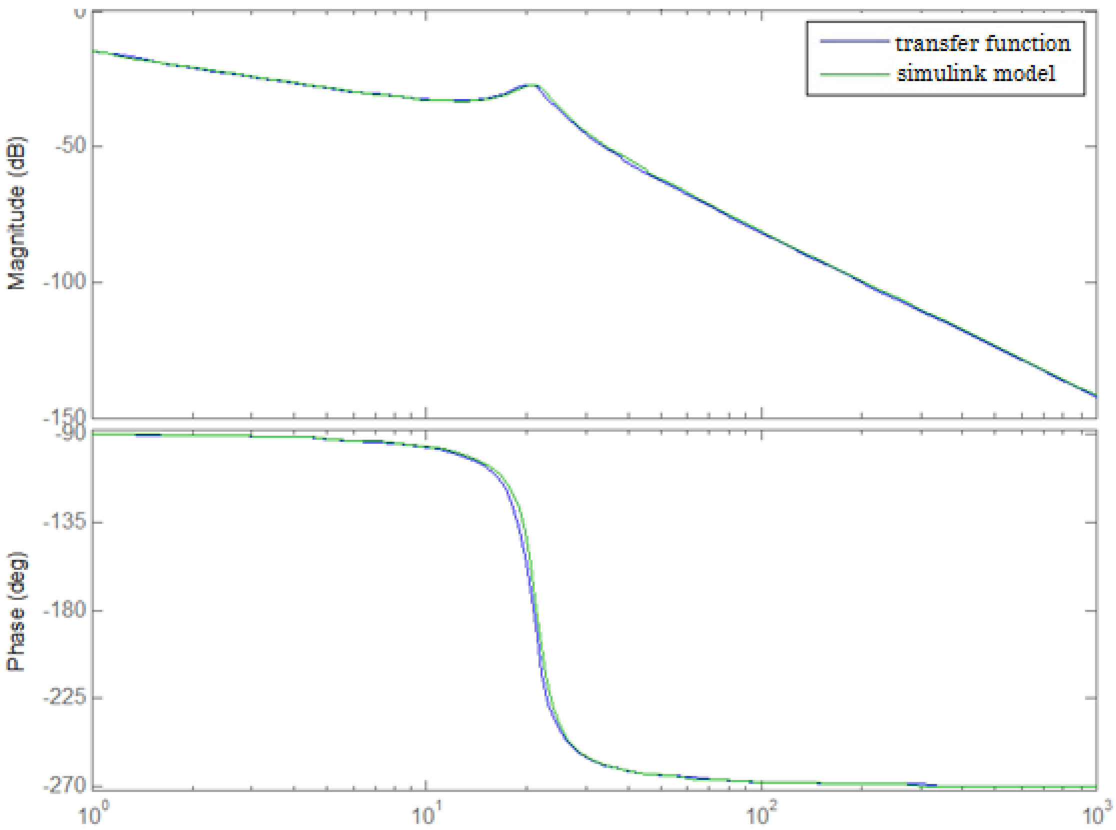

Figure 12 - Bode plot comparison between transfer function and Simulink motor model.

3.5 Example rotational system

Figures 13 and 14 show some simulation results of the rotational heave compensation system. Figure 13 shows the flow behaviour through the proportional four-way valve. When the vessel rises the cable length needs to be extended, so the motor turns in negative direction. This corresponds to a positive flow q_2 and a negative flow q_1 and vice versa. In comparison to the translational system the fluid flows q_1 and q_2 are of the same magnitude, because the volumes V_1 and V_2 were assumed equal in paragraph 3.4. Figure 10 shows the pressures in motor at entry side 1 and 2, respectively.

The heave motion of the vessel will introduce a dynamic force in the cable that results in a displacement of the load. The four-way valve will regulate the flow in and out of the motor to generate a torque that rotates the drum in counter phase with the heave motion. The fact that there is more fluctuation in the pressure lines of the motor than there is in figure 10 of the cylinder, even though both simulations were performed under the exact same conditions, suggests that the rotational system has more difficulties compensating for the heave motion than the translational system. This is due to the fact that the rotational system has to rotate a much larger inertia of all the spare cable on the drum.

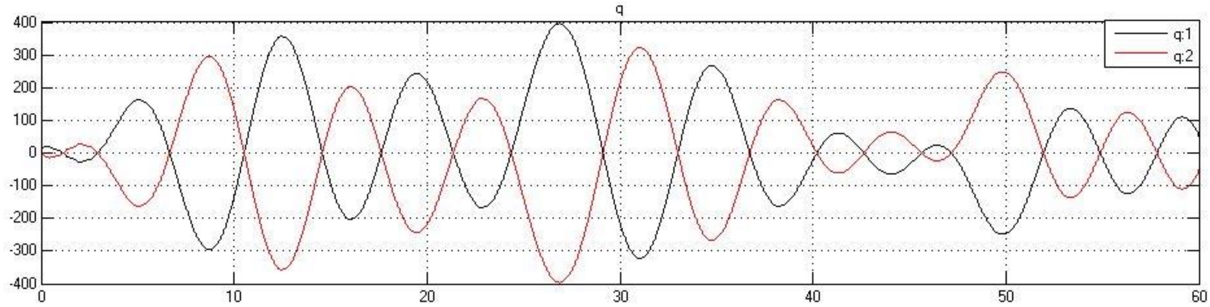

Figure 13 – Fluid flow q_1 and q_2 [L/min] from four-way valve to motor entry side 1 and 2, respectively, vs time [s].

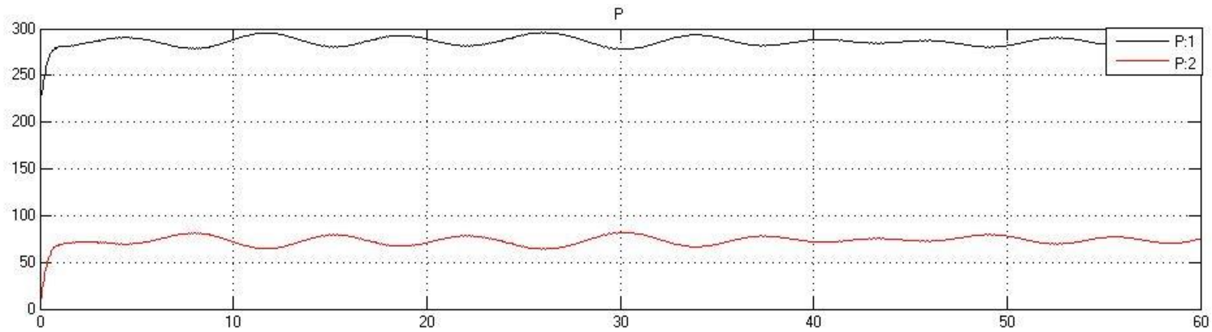

Figure 14 – Pressures [Bar] at motor entry side 1 and 2, respectively, versus time [s].

4 Passive heave compensation

Chapter 3 briefly mentioned the possibility to extend the active heave compensation system with a passive heave compensation system by means of a nitrogen accumulator unit. In general this is only applied for the translational systems as it is relatively easy to add a passive cylinder, see figure 15.

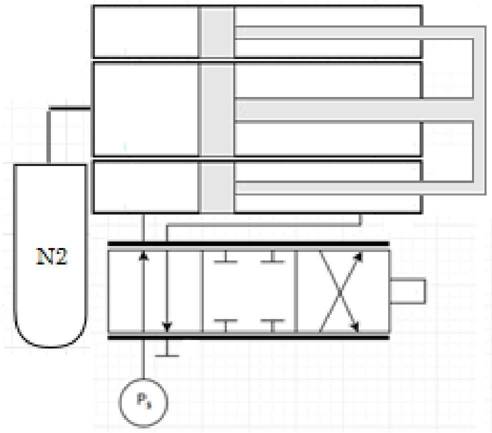

Figure 15 – Translational system expanded with an accumulator unit.

The passive cylinder reliefs the system of static forces, which offers the opportunity to reduce the active cylinders in size to increase efficiency. Also the system can be applied on a broader range of operating conditions as the pressure inside the accumulator can be set to match the given load case.

4.1 Nitrogen Accumulator

Figure 16 regards the nitrogen accumulator unit as a cylinder that is divided into two pressure chambers by a piston. The top chamber is filled with nitrogen gas at high pressure, the bottom chamber is filled with oil. The dimensions of the chambers are fully dependent of the position of the piston x_p. There is no fluid flow at the top side of the accumulator, volume change due to piston displacement will either compress or expand the nitrogen gas resulting in pressure differences.

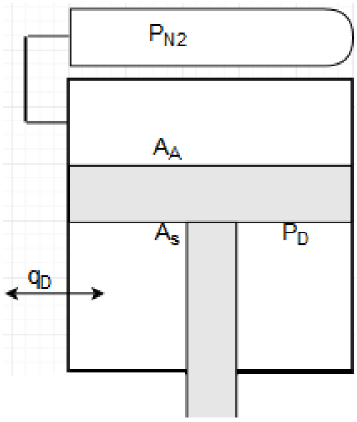

Figure 16 - Schematic view nitrogen accumulator.

The volume flow q_D at the bottom side of the cylinder depends on the displacement of the piston $\dot{x}_p$ and the compressibility of the oil, according to equation 4.1 (assuming no leakage inside the cylinder).

$$q_D = \frac{V_t}{\beta}\dot{p}_D + A_s\dot{x}_p \tag{4.1}$$

4.2 Ideal gas equation

The pressure at the topside of the accumulator (figure 16) can, under certain circumstances, be described by the ideal gas equation, given in equation 4.2.

$$pv = RT \tag{4.2}$$

With pressure p, specific volume v, gas constant R and temperature T. The gas constant depends on the specified gas and can be calculated using equation 4.3.

$$R = \frac{R_u}{M} \tag{4.3}$$

With R_u the universal gas constant and M the molar mass of the specified gas. Substitution in 4.2 gives equation 4.4.

$$pvM = R_u T \tag{4.4}$$

Name	Variable	Value	Unit
Critical pressure	p_{cr}	33.9	$[Bar]$
Critical temperature	T_{cr}	126.2	$[Kelvin]$
Critical density	ρ_{cr}	311.60	$\left[\frac{kg}{m^3}\right]$
Molar mass	M	$28.013 \cdot 10^{-3}$	$\left[\frac{kg}{mol}\right]$
Universal gas constant	R_u	8.314	$\left[\frac{Pa \cdot m^3}{mol \cdot Kelvin}\right]$

Table 3 – Properties for nitrogen gas[10].

Nitrogen can be considered an ideal gas under the following circumstances:

$$\frac{p}{p_{cr}} \ll 1\,, \qquad \frac{T}{T_{cr}} > 2 \qquad \rightarrow \qquad p \ll 33.9\ [bar], \qquad T > 252.4\ [K] \tag{4.5}$$

The conditions inside the accumulator are in line with the temperature criterion, but the pressure will be well above 33.9 bar. In that case the ideal gas equation will give poor results and proper description of the compressibility of nitrogen gas requires a more complicated model.

4.3 Bender equation of state

To get a proper description of the behaviour of nitrogen gas inside the accumulator the Bender equation of state is used, given by equation 4.6. The bender equation of state expands the ideal gas equation with 20 constants in order to give an accurate description of the behaviour of a gas up to a pressure and temperature of 1000 bar and 2000 Kelvin, respectively [10].

$$p = \rho T\left(R + B\rho + C\rho^2 + D\rho^3 + E\rho^4 + F\rho^5 + (G + H\rho^2)\rho^2 e^{-n_{20}\rho^2}\right) \tag{4.6}$$

$$B = n_1 + \frac{n_2}{T} + \frac{n_3}{T^2} + \frac{n_4}{T^3} + \frac{n_5}{T^4} \qquad C = n_6 + \frac{n_7}{T} + \frac{n_8}{T^2}$$

$$D = n_9 + \frac{n_{10}}{T} \qquad E = n_{11} + \frac{n_{12}}{T}$$

$$F = \frac{n_{13}}{T} \qquad G = \frac{n_{14}}{T^3} + \frac{n_{15}}{T^4} + \frac{n_{16}}{T^5}$$

$$H = \frac{n_{17}}{T^3} + \frac{n_{18}}{T^4} + \frac{n_{19}}{T^5}$$

Taking $\alpha = -n_{20}$, equation 4.6 becomes a linear function with 19 coefficients. The coefficients can be made dimensionless using the following ratios (Rotthäuser, 1993).

$$\omega = \frac{v_{cr}}{v} = \frac{\rho}{\rho_{cr}}, \qquad \tau = \frac{T_{cr}}{T} \tag{4.7}$$

Substitution of 4.7 into 4.6 gives equation 4.8 (Rotthäuser, 1993).

$$p = \frac{RT}{v}\left[1 + \sum_{i=1}^{19} B_i Y_i\right] \tag{4.8}$$

This equation looks much the ideal gas equation of equation 4.2, where the sum $\sum_{i=1}^{19} B_i Y_i$ accounts for the non-ideal behaviour of the nitrogen gas. The coefficients B_i and Y_i are given in table 4 [10].

i	B_i	Y_i			
1	$5.1564398 \cdot 10^{-1}$	ω	11	$-2.7239453 \cdot 10^{-2}$	ω^4
2	$-1.2350862 \cdot 10^{0}$	$\omega\tau$	12	$1.2113829 \cdot 10^{-1}$	$\omega^4\tau$
3	$-3.3660701 \cdot 10^{-2}$	$\omega\tau^2$	13	$1.2924526 \cdot 10^{-2}$	$\omega^5\tau$
4	$-4.3693391 \cdot 10^{-1}$	$\omega\tau^3$	14	$-3.2495834 \cdot 10^{-1}$	$\omega^2\tau^3 e^{\alpha\omega^2}$
5	$6.1598645 \cdot 10^{-2}$	$\omega\tau^4$	15	$5.3924336 \cdot 10^{-1}$	$\omega^2\tau^4 e^{\alpha\omega^2}$
6	$5.2599330 \cdot 10^{-2}$	ω^2	16	$-2.0692385 \cdot 10^{-1}$	$\omega^2\tau^5 e^{\alpha\omega^2}$
7	$2.0756488 \cdot 10^{-1}$	$\omega^2\tau$	17	$-1.5625825 \cdot 10^{-1}$	$\omega^4\tau^3 e^{\alpha\omega^2}$
8	$2.0273530 \cdot 10^{-1}$	$\omega^2\tau^2$	18	$5.2222667 \cdot 10^{-1}$	$\omega^4\tau^4 e^{\alpha\omega^2}$
9	$2.3974975 \cdot 10^{-1}$	ω^3	19	$-3.8027769 \cdot 10^{-2}$	$\omega^4\tau^5 e^{\alpha\omega^2}$
10	$-4.7905077 \cdot 10^{-1}$	$\omega^3\tau$	α	-0.9641	

Table 4 - Coefficients B_i and Y_i in the Bender equation of state[10].

The derivative of pressure p with respect to temperature T is given in equation 4.9. This equation is required in the gas temperature model in paragraph 4.4.

$$\begin{aligned}\frac{\partial p}{\partial T} = -\frac{R}{T^5 v}\big(&-T^5 - B_1\omega T^5 - B_6\omega^2 T^5 - B_9\omega^3 T^5 - B_{11}\omega^4 T^5 + 4B_{16}\omega^2 T_{cr}^5 e^{\alpha\omega^2} \\ &+ 4B_{19}\omega^4 T_{cr}^5 e^{\alpha\omega^2} + B_3\omega T_{cr}^2 T^3 + 2B_4\omega T_{cr}^3 T^2 + 3B_5\omega T_{cr}^4 T \\ &+ B_8\omega^2 T_{cr}^2 T^3 + 2B_{14}\omega^2 T_{cr}^3 e^{\alpha\omega^2} T^2 + 3B_{15}\omega^2 T_{cr}^4 e^{\alpha\omega^2} T \\ &+ 2B_{17}\omega^4 T_{cr}^3 e^{\alpha\omega^2} T^2 + 3B_{18}\omega^4 T_{cr}^4 e^{\alpha\omega^2} T\big)\end{aligned} \tag{4.9}$$

4.4 Gas temperature model

The gas side of the accumulator of figure 16 is considered a closed system where no change in mass can occur, but there will be change in energy. The first law of thermodynamics states that energy can neither be created nor destroyed, but can change form.

$$\dot{Q}_{conv} - \dot{W} = \dot{U} \tag{4.10}$$

The change of internal energy $\dot{U}$ equals the change of heat $\dot{Q}$ minus the work $\dot{W}$. The change of heat can be calculated using equation 4.11.

$$\dot{Q}_{conv} = hA(T_a - T) \tag{4.11}$$

Where h is the convection heat transfer coefficient, A is the respective area, T_a and T are the ambient temperature and gas temperature, respectively.

The work done depends on the change of volume as in equation 4.12.

$$\dot{W} = p\frac{dV}{dt} \tag{4.12}$$

The internal energy of real gases can be calculated using equation 4.13.

$$\dot{U} = mC_v\frac{dT}{dt} + m\left(T\left(\frac{\partial p}{\partial T}\right)_v - p\right)\frac{dV}{dt} \tag{4.13}$$

Substitution of equations 4.11-4.13 into the first law of thermodynamics yields equation 4.14.

$$hA_w(T_a - T) - p\frac{dV}{dt} = m_{gas}C_v\frac{dT}{dt} + m_{gas}\left(T\left(\frac{\partial p_{gas}}{\partial T}\right)_v - p_{gas}\right)\frac{dv}{dt} \tag{4.14}$$

Rearranging process (4.15 - 4.21) transforms equation 4.14 into equation 4.21:

$$hA_w(T_a - T) - p_{gas}\frac{dV}{dt} = m_{gas}C_v\frac{dT}{dt} + \left(m_{gas}T\left(\frac{\partial p_{gas}}{\partial T}\right)_v - m_{gas}p_{gas}\right)\frac{dv}{dt} \tag{4.15}$$

$$hA_w(T_a - T) - p_{gas}\frac{dV}{dt} = m_{gas}C_v\frac{dT}{dt} + m_{gas}T\left(\frac{\partial p_{gas}}{\partial T}\right)_v\frac{dv}{dt} - m_{gas}p_{gas}\frac{dv}{dt} \tag{4.16}$$

$$hA_w(T_a - T) - p_{gas}\frac{dV}{dt} = m_{gas}C_v\frac{dT}{dt} + m_{gas}T\left(\frac{\partial p_{gas}}{\partial T}\right)_v\frac{dv}{dt} - p_{gas}\frac{dV}{dt} \tag{4.17}$$

$$hA_w(T_a - T) = m_{gas}C_v\frac{dT}{dt} + m_{gas}T\left(\frac{\partial p_{gas}}{\partial T}\right)_v\frac{dv}{dt} \tag{4.18}$$

$$m_{gas}C_v\frac{dT}{dt} = hA_w(T_a - T) - m_{gas}T\left(\frac{\partial p_{gas}}{\partial T}\right)_v\frac{dv}{dt} \tag{4.19}$$

$$\frac{dT}{dt} = \frac{hA_w}{m_{gas}C_v}(T_a - T) - \frac{m_{gas}}{m_{gas}C_v}T\left(\frac{\partial p_{gas}}{\partial T}\right)_v\frac{dv}{dt} \tag{4.20}$$

$$\frac{dT}{dt} = \frac{(T_a - T)}{\tau} - \frac{T}{C_v}\left(\frac{\partial p_{gas}}{\partial T}\right)_v\frac{dv}{dt} \tag{4.21}$$

With τ being the thermal time constant, calculated with equation 4.22.

$$\tau = \frac{mC_v}{hA} \tag{4.22}$$

Where m is the mass of the nitrogen, C_v is the specific heat capacity of nitrogen, h is the convection heat transfer coefficient and A is the respective area.

4.5 Simulink model

The gas pressure and temperature models are combined so that the pressure of the nitrogen gas can be described as a function of the piston displacement. An example of the pressure behaviour of the nitrogen gas in [Pa] versus the piston position in [m] can be found in figure 17. Note that the position of the piston is scaled with a factor 10^7. In this example the piston has a maximum stroke of 3 meters and is initially balanced at its centre position. The volume of the accumulator is five times bigger than the volume inside the cylinder to make the change in pressure less aggressive as the piston moves to compensate for heave motion.

Figure 17 corresponds to the volumes: $V_c = A \cdot x \approx 0.04\, m^3 \rightarrow V_{N2} = 0.20\, m^3$.

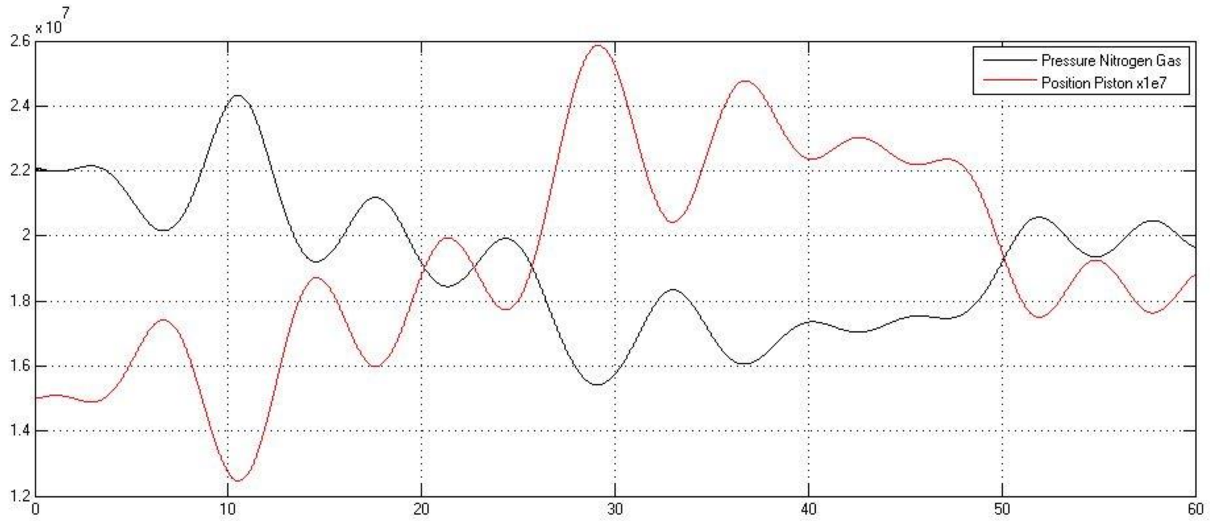

Figure 17 – Pressure of nitrogen gas [Pa] and piston position [m] versus time [s].

5 Controller design

The four-way proportional valve requires a controller to regulate the flow that is delivered to the actuator, which can be a cylinder or a motor. The input signal for the valve is between $\pm 10\ V$. The system is controlled with a proportional-derivative controller with velocity feedforward, in the form:

$$x_v = \dot{r} + K_p(r - q) + K_d(\dot{r} - \dot{q}) \tag{5.1}$$

Velocity feedforward from the motion reference unit is applied, making the configuration q exactly trace reference signal r. The feedback controller is used to stabilise the system, which is needed because the system is only marginal stable. Furthermore, feedback is needed to counteract unknown disturbances and cope with small errors in the model.

The transfer function of the valve opening over the respective actuator displacement was given earlier in equations 3.18 and 3.28. A more general description of the plant is given in equation 5.2 [7].

$$P(s) = \frac{K_v}{\left(1 - \frac{s}{\omega_t}\right) s \left(1 + 2\zeta_h \frac{s}{\omega_h} + \frac{s^2}{\omega_h^2}\right)} \tag{5.2}$$

The critical parameter in this servo system is the amplitude margin A_m, which is expressed as:

$$A_m = -20^{10} \log \left| \left(\frac{K_v}{-2\zeta_h \omega_h} \right) \right| \ [\mathrm{dB}] \tag{5.3}$$

In other words, the control system will be stable if the amplitude margin is positive, which gives the stability criteria as [7]:

$$K_v < 2\zeta_h \omega_h \tag{5.4}$$

With hydraulic damping coefficient ζ_h and hydraulic resonance frequency ω_h defined in equations 4.19 and 4.29. Figure 18 shows the bode plot response of the hydraulic cylinder with PD-control.

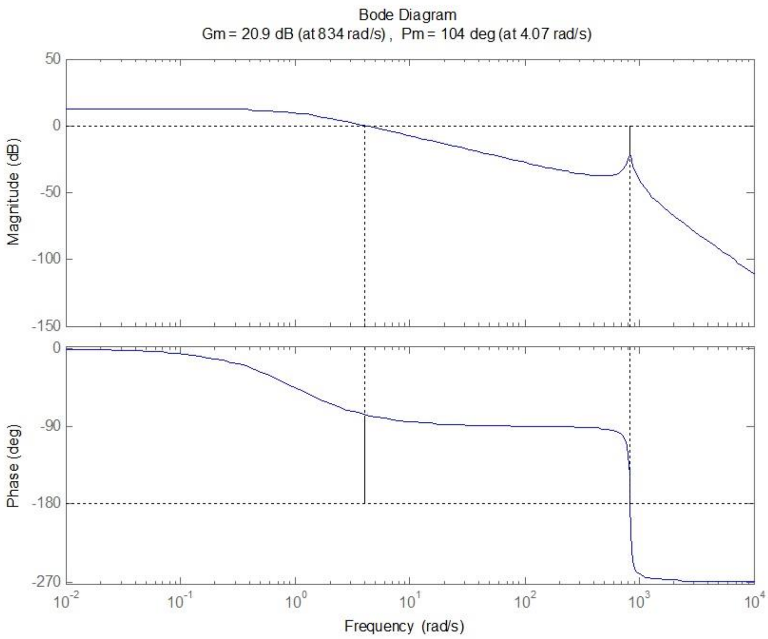

Figure 18 – Bode plot of the hydraulic cylinder and four way valve with PD-controller.

5.1 Velocity feedforward

The velocity of the crane tip is measured in the motion reference unit and used to derive the required actuator velocity to counter the heave motion of the vessel, see equation 5.5.

$$v_{actuator} = -\frac{v_{heave}}{i} \tag{5.5}$$

The variable i denotes the ratio between the velocity heave motion and the velocity of the actuator. This is a constant factor 2 for the translational system, because the cable is guided over sheaves around the cylinder. In the rotational system this ratio equals the radius of the drum, which depends on the amount of cable on the drum.

The desired actuator velocity can then be used to determine the required flow rate between the actuator and the four-way valve, as in equation 5.6 for the translational and rotational system, respectively.

$$Q = \frac{A_p v_p}{\eta_v} \quad \text{or} \quad Q = \frac{D_m \omega_m}{\eta_v} \tag{5.6}$$

The required flow can be multiplied with the inverse description of the valve as in equation 5.7.

$$U(V) = \frac{Q}{C_d b \sqrt{\frac{2\Delta p}{\rho}}} \tag{5.7}$$

The velocity feedforward loop send the exact voltage to the four-way valve to achieve the required flowrate for compensating for the measured heave motion of the vessel.

5.2 Tension feedback

As described in paragraph 2.1 the length of the cable is reversely proportional to the cable stiffness. Increasing operating depths result in a more significant oscillations of the load at the bottom of the cable. This greatly reduces the overall accuracy of the system since the position error of the controller is measured at the crane tip and does not account for it. Figure 19 shows the remaining error measured in the crane tip versus the remaining position error measured in the load. The simulation is performed with a 17.5 ton load at 3000m operating depth in the cylinder configuration.

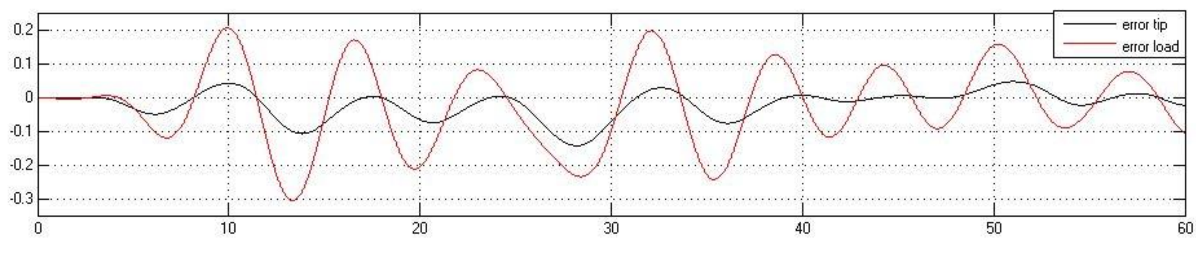

Figure 19 – Error of the crane tip and error of the load [m] versus time [s].

Figure 19 shows that there is indeed a significant difference between the remaining position error of the tip and load. Therefore, a control method is introduced to reduce the oscillatory motion of the load. The oscillations originate from the force fluctuations in the cable that are caused by external disturbances. Assuming the tension in the cable is measured, one can compensate for the static forces like gravity.

$$\Delta F_{dyn} = F_{cable} - F_{static} \tag{5.8}$$

The next step would be to derive the effect of these force fluctuations on the motion of the actuator, assuming the system is initially at rest.

$$\begin{aligned} \sum F &= \quad 2 \cdot \Delta F_{dyn} = m_p a_p \\ \sum T &= \frac{D_{dr}}{2} \cdot \Delta F_{dyn} = J_m \alpha_m \end{aligned} \tag{5.9}$$

Having determined the effects of the force fluctuations in the cable on the respective accelerations of the actuator, the corresponding actuator velocity can be derived. This velocity can then be countered through the velocity feedforward loop of paragraph 5.1. Figure 20 shows the effect of tension feedback on the errors of the tip and load under the exact same circumstances as in figure 19. The reduction in oscillating behaviour increases the stability and accuracy of the system.

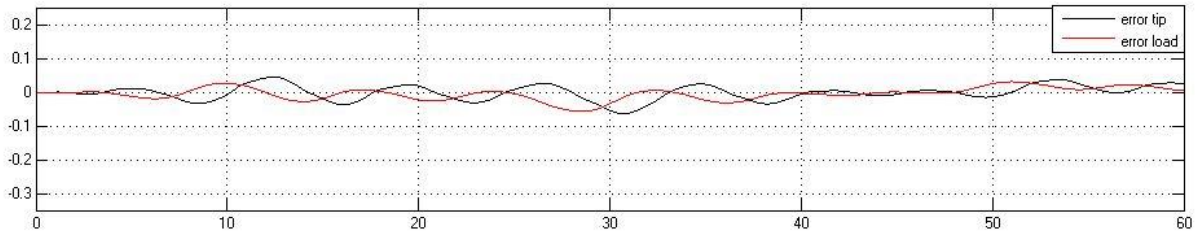

Figure 20 – Error of the crane tip and error of the load [m] versus time [s], with tension feedback.

6 Model Validation

The translational and rotational hydraulic systems were validated in figures 8 and 12 in Chapter 3, by comparing their bode plot responses with the responses of corresponding transfer functions found in literature. This gives a proper insight on the level correctness regarding the Simulink models of the hydraulic components. The complete Simulink model also contains the dynamics of the hoisting mechanism, the equation of motion of the load and a description of ocean waves that result in the heave motion itself that require validation. It would also be good to get an insight on the capabilities of the controller developed in Chapter 5. This is achieved by comparing the model to a practical application best suiting this report, that is still in use these days. This would be a heave compensation system HYCOM B.V. delivered for TMS, see figure 21.

Figure 21 – Knuckle boom crane TMS aboard the Up Coral.

A heave compensation system was designed for the winch of a knuckle boom crane, capable of placing a 30 ton load up to an operating depth of 3000 meter. The delivered hydraulic system corresponds to the rotational system described in paragraph 3.4, see figure 22. The specifications regarding the dimensions of the hydraulic system, cable and drum are given in table 5.

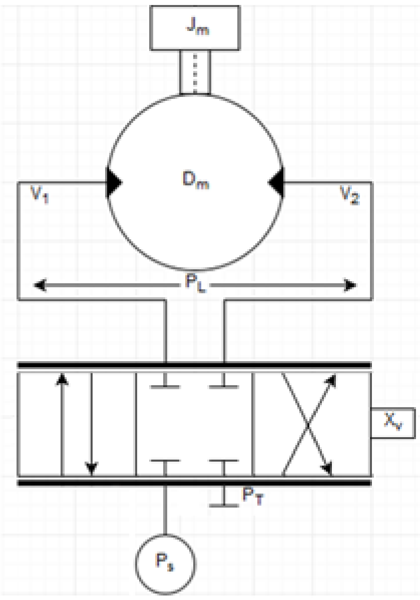

Figure 22 – Schematic rotational heave compensation system.

Mass load (underwater and including cable) Motor stroke volume Max flow capacity Max power	m_l D_m Q_m P_{max}	$30\ ton$ $23\ L/rad$ $2000\ L/min$ $750\ kW$
Cable diameter Drum diameter empty Drum diameter full layer Inertia empty drum Inertia full layer drum	d_c d_D d_{Dr} J_{d_0} J_d	$0.034\ m$ $2.6\ m$ $3\ m$ $3e4\ kg \cdot m^2$ $6e4\ kg \cdot m^2$

Table 5 – Specifications heave compensation system in TMS crane.

The heave compensation system described above is applied on the TMS crane. In practice this heave compensation system has achieved an accuracy of $\pm 30\ cm$ measured in the position of the load at an operation depth of 3000 meter. This accuracy was achieved using a controller with a proportional-derivative feedback loop. The error was measured during the testing phase using a RV that was positioned down at the sea bed. This made it possible to get an insight on the displacement of the load, whereas normally the displacement of the crane tip is measured.

The specifications as given in table 5 have been implemented in the model of the rotational heave compensation system that corresponds to figure 22. The performance of the rotational system has been simulated in the case of a proportional-derivative controller and in case of the controller with velocity feedforward and tension feedback, designed in Chapter 5.

Both controllers are subjected to the heave motion shown in figure 23. The simulation results for a simple PD-controller are shown in figures 24-26. The results of the controller designed in Chapter 5 are shown in figures 27-29.

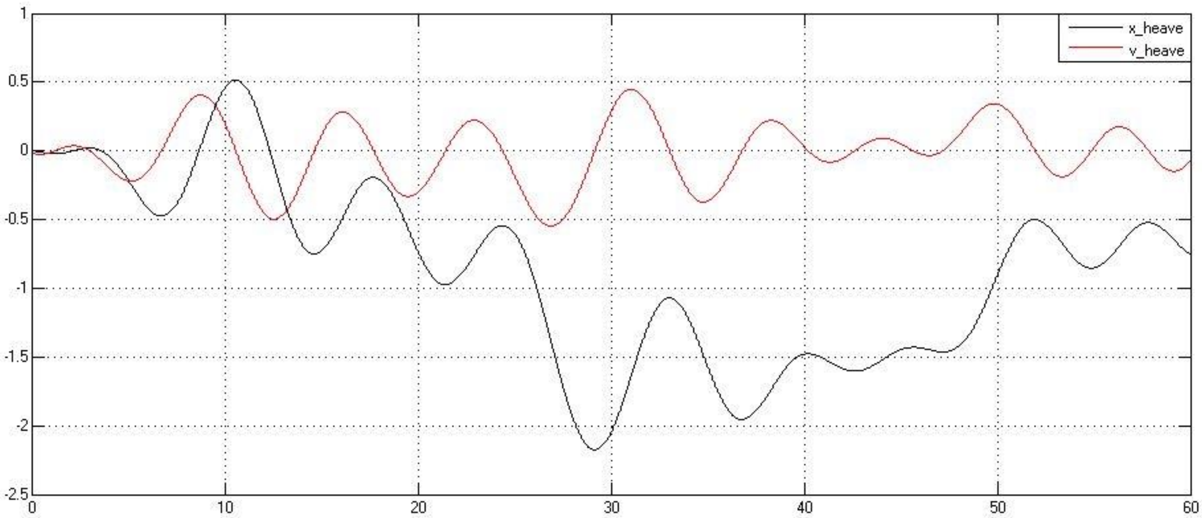

Figure 23 – Heave motion in the crane tip, position in [m] and velocity in [m/s] versus time [s].

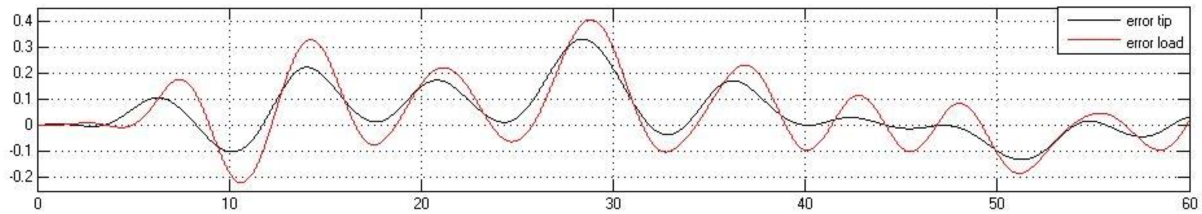

Figure 24 – Position errors of the crane tip and load in [m] versus time in [s] for PD-control.

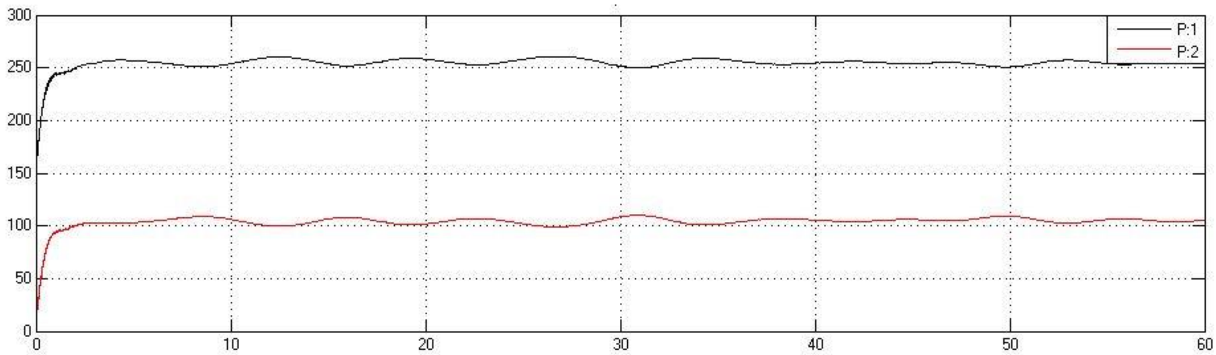

Figure 25 – Pressure behaviour of the hydraulic motor unit in [bar] versus time in [s].

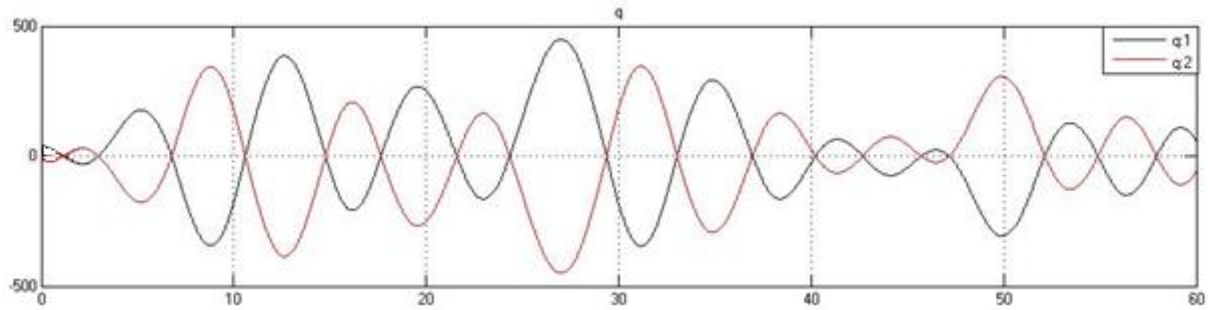

Figure 26 – Flows q_1 and q_2 from four-way valve to hydraulic motor in [L/min] versus time in [s].
Power consumption of the pump: 1.43 kWh.

Figure 24 shows a position error of the load between $40\ cm$ and $-20\ cm$. This does not exactly correspond to the situation the heave compensation system of the TMS crane encountered in practice ($\pm 30cm$), but that would be impossible as the model is subjected to a random heave motion. The fact that the error is of the same order concludes that the Simulink model gives a realistic view of the performance of the heave compensation system at an operating depth of 3000 meter. At the operating depth of 3000 meter the dynamic behaviour of the cable has significant influence on the error of the load. This indicates that the relatively simple cable model that places half the cable mass at the load and the other half at the crane tip is sufficient for describing its influence on the motion of the load.

Interesting to see is the performance of the controller designed in Chapter 5 and especially the influence of the tension control to get a measure of improvement with respect to performance of a practical application. Figures 27-28 show simulation results using the advanced controller with velocity feedforward and tension feedback, subjected to the same heave motion from figure 23.

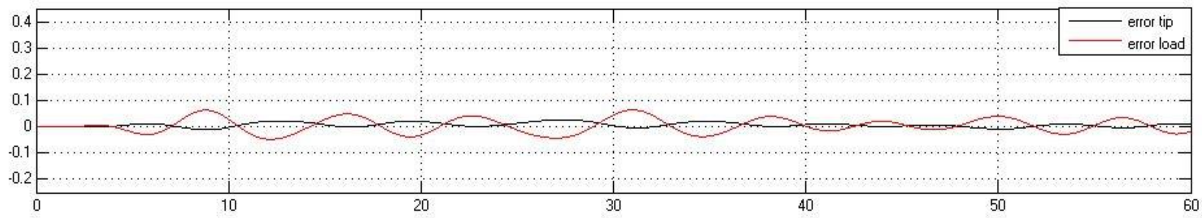

Figure 27 – Position errors of the crane tip and load in [m] versus time in [s] with advanced controller.

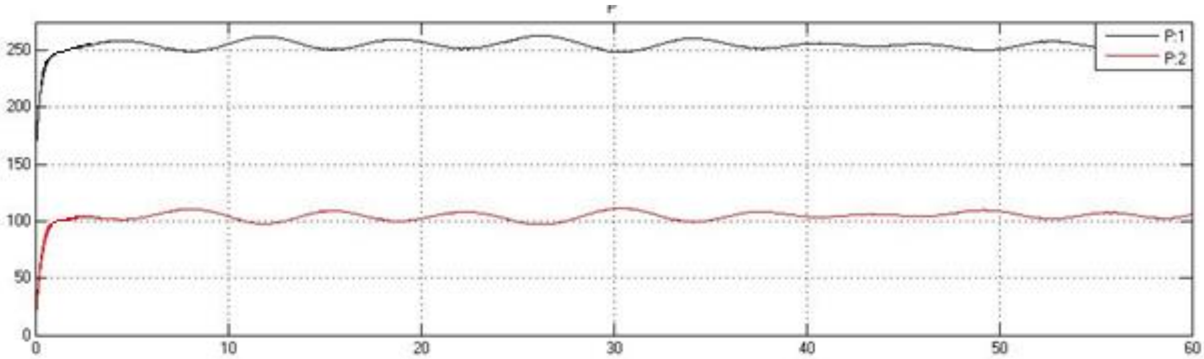

Figure 28 – Pressure behavior of the hydraulic motor unit in [bar] versus time in [s].

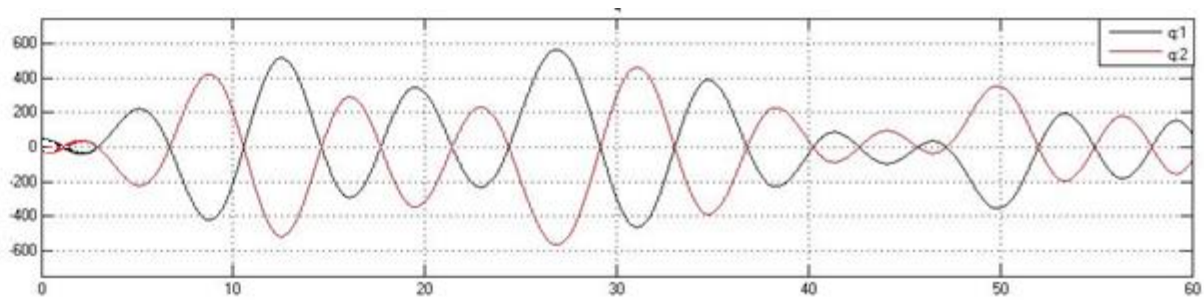

Figure 29 – Flows q_1 and q_2 from four-way valve to hydraulic motor in [L/min] versus time in [s].
Power consumption of the pump: 1.82 kWh.

Comparing figure 27 to figure 24 makes clear that velocity feedforward and tension feedback control reduces the error of both the crane tip and the load significantly. The errors of the crane tip and the load are intertwined. Velocity feedforward has most influence on the error of the crane tip, while tension control is used to supress the oscillatory motion of the load.

The error of the crane tip reduces from $\begin{pmatrix} +\,0.30 \\ -\,0.10 \end{pmatrix}$ in figure 24 to $\begin{pmatrix} +\,0.03 \\ -\,0.03 \end{pmatrix}$ in figure 27.
The error of the load is reduced from $\begin{pmatrix} +\,0.40 \\ -\,0.20 \end{pmatrix}$ in figure 24 to $\begin{pmatrix} +\,0.07 \\ -\,0.07 \end{pmatrix}$ in figure 27.
In case only velocity feedforward was used the error of the crane tip remains at $\begin{pmatrix} +\,0.03 \\ -\,0.03 \end{pmatrix}$, but the unsuppressed oscillatory motion of the load then results in an error of the load of $\begin{pmatrix} +\,0.15 \\ -\,0.15 \end{pmatrix}$.

The situation sketched in figures 24-26 correspond to a situation encountered in practice with the TMS crane. This makes it safe to say that the simulation gives a proper approximation of the performance of the heave compensation system. Which suggests that the improvement in performance that is achieved by using velocity feedforward and tension control in figures 27-29 is also a proper indication of what is realisable in practice.

7 Simulation results

The hydraulic components were validated in Chapter 3 with respect to corresponding transfer functions. In Chapter 6 the complete Simulink assembly was validated by comparing simulation results with test results from a practical application. This chapter continues on the results of Chapter 6 by comparing the performance and efficiency for the theoretical case that a translational system was used rather than a rotational system. To make a fair comparison both systems are specifically redesigned for the testing conditions of the TMS project.

7.1 Approach

Two hydraulic heave compensation systems with translational and rotational actuation, respectively, are shown in figure 30. The dimensions of both systems are determined for the testing conditions of the TMS project in Chapter 6. The load attached to the cable has a mass of $m_l = 30$ ton and the maximum operating depth is 3000 meter.

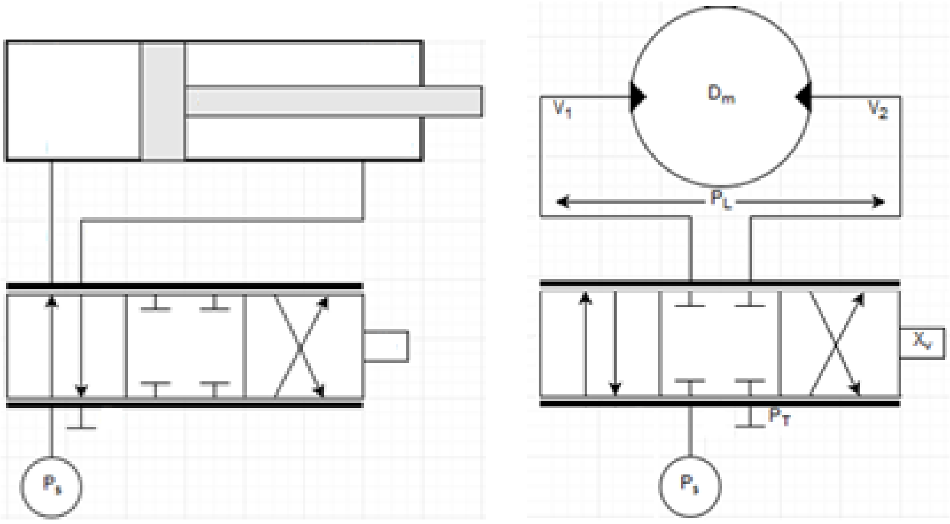

Figure 30 – Translational and rotational heave compensation systems, respectively.

Hydraulic cylinder	Hydraulic motor
$m_l = 30$ ton	$m_l = 30$ ton
$i = 2$	$i = D_{dr}/2$
$F_l = 624$ kN	$T_l = 411$ kNm
$D = 0.190$ m	$D_m = 18$ L/rad
$Q_{pump} = 1400$ L/min	$Q_{pump} = 1400$ L/min
$P_{pump} = 575$ kW	$P_{pump} = 575$ kW

Table 6 – Actuator dimensions of the hydraulic cylinder and motor, respectively.

In table 6 the variable i denotes the ratio between the tension in the cable and the force or torque experienced by the actuator. For the translational system this ratio is 2, because the cable is guided over sheaves around the cylinder. In the rotational system this ratio equals the radius of the drum, which depends on the amount of cable on the drum. The diameter of the empty drum is 2.6 meter. A full drum contains 3000 meter of cable, the diameter of a full drum is approximately 3 meters. The ratio i also relates the actuator velocity to the cable velocity, which works through on the required pump installation for the two systems.

Simulations are performed for varying load cases in paragraph 7.2. Performance is measured in remaining position errors of the crane tip and the load. Efficiencies can be compared by the power consumption of the pump noted in kWh beneath every graph. The heave compensation systems will be subjected to the same heave pattern for all simulations, shown in figure 31.

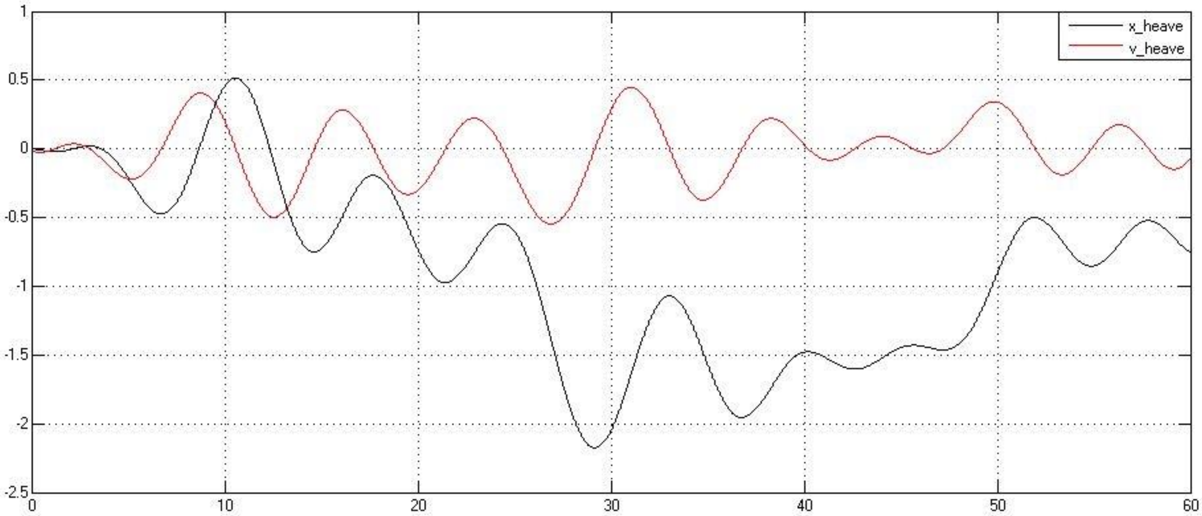

Figure 31 - Heave motion in the crane tip, position in [m] and velocity in [m/s] versus time [s].

7.2 System performance

7.2.1 Load case 1

Operating depth: $L_c = 3000$ m.
Mass of the load: $m_l = 30$ ton.
Mass of the cable: $m_c = 12$ ton.

Figures 32 and 33 show the simulation results for the situation sketched in table 6 for load case 1. The operating depth is 3000 meters, the combined mass of load and cable equals $m_{tot} = 36$ ton as only half the cable mass is placed directly on the load. Considering buoyancy forces the equivalent mass becomes about $m_{eq} \approx 31$ ton.

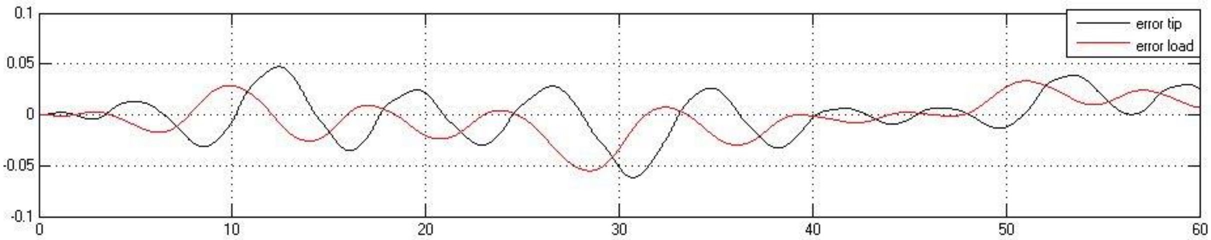

Figure 32 – Error of the crane tip and error of the load [m] versus time [s] for translational system. Power consumption of the pump: 1.26 kWh.

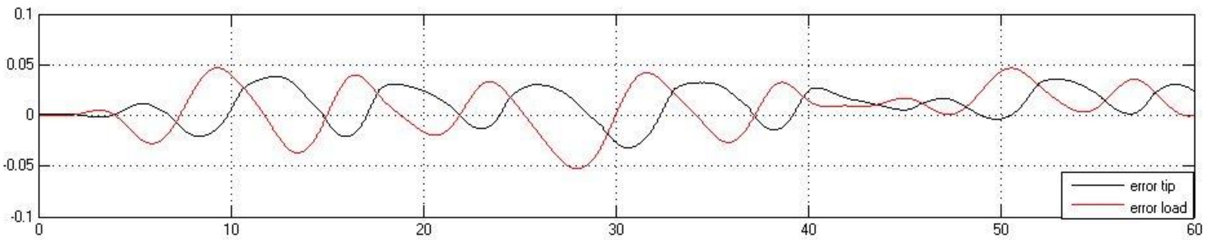

Figure 33 – Error of the crane tip and error of the load [m] versus time [s] for rotational system. Power consumption of the pump: 1.46 kWh.

Figures 32 and 33 show the performance of translational and rotational heave compensation systems in terms of remaining errors of the crane tip and the load. The errors of both systems are of the same order, while the efficiency in terms of power consumption of the pump is about 14% better in case of the translational system with respect to the rotational system. This was expected as table 6 shows that the rotational system requires a larger pump installation for the same operating conditions.

An interesting observation in figures 32 and 33 is that the translational system seems to achieve a higher accuracy of the load, whereas the accuracies are of the same order for the rotational system. This seems odd as the cable and load model for the two setups is exactly the same. This can be observed in figures 34 and 35 that show the performance of both systems without tension control.

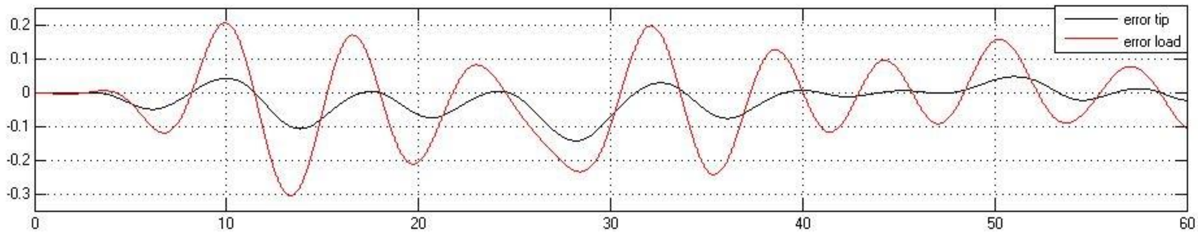

Figure 34 – Performance of the translational system without tension control.

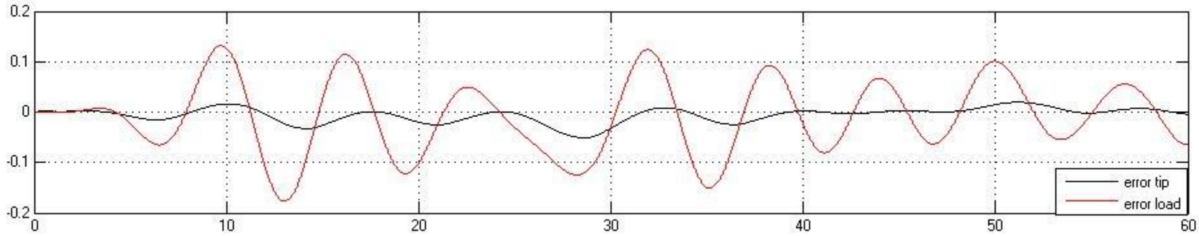

Figure 35 – Performance of the rotational system without tension control.

Figures 34 and 35 show the same response for both systems. The error of the load has increased with respect to figures 32-33 ($\epsilon = \pm 15$cm), but the error of the crane tip is significantly smaller. This can be explained by considering the feedforward loop with respect to the tension control loop.

The velocity feedforward loop calculates the respective actuator velocity that is required to counter the measured velocity of the crane tip. The actuator velocity leads to the required flow rate that can be multiplied with the inverse of the four-way valve which results in the input voltage for the valve. This principle has been extensively described in Chapter 5. Tension control uses the same feedforward loop, but to counter the unwanted dynamics that originate from the oscillatory motion of the load.

These are two entirely different motions with different phase and frequency and may therefore counter each other, as can be seen in figure 36. The feedforward loops for the two actuation systems depend on the respective system, which explains the different responses with respect to tension control in figures 32 and 33.

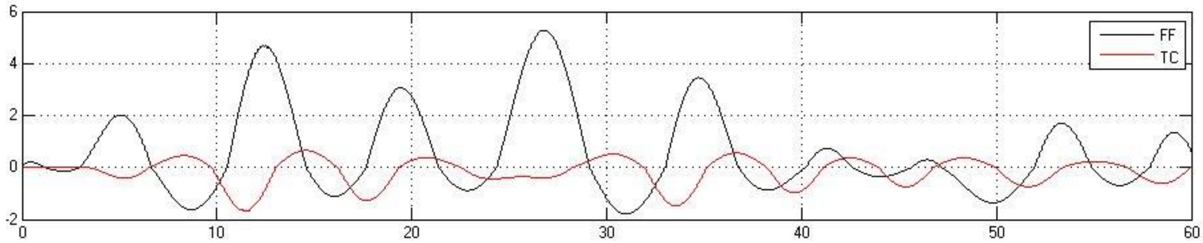

Figure 36 – Controller output in [V] versus time [s] of feedforward and tension control, respectively.

Figure 36 shows that countering the oscillatory motions of the load with tension control may not always be beneficial to the velocity feedforward loop. The feedforward loop is used to counter the heave motion in the crane tip. This means the measured and visible error of the crane tip might increase, while the position error of the load underwater decreases.

7.2.2 Load case 2

Operating depth: $L_c = 100$ m.
Mass of the load: $m_l = 30$ ton.
Mass of the cable: $m_c = 0.4$ ton.

Load case 2 considers the same systems at an operating depth of 100 meter. At this point the mass of the cable is negligible with respect to the mass of the load, so the system can be considered over-dimensioned. Figures 37 and 38 show the performance of both systems under these operating conditions.

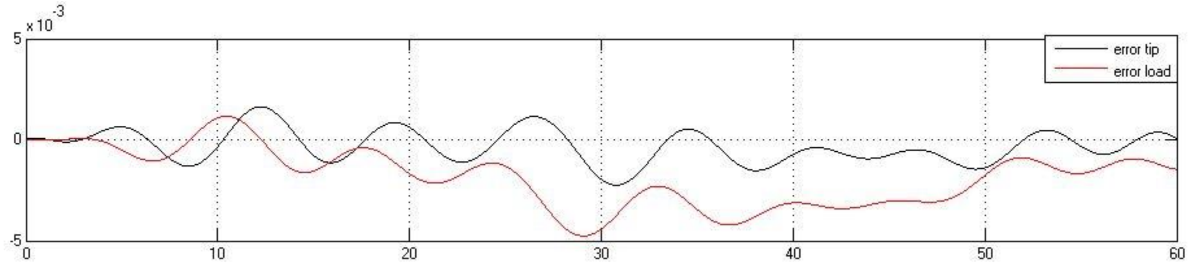

Figure 37 – Error of the crane tip and error of the load [m] versus time [s] for translational system. Power consumption of the pump: 1.25 kWh.

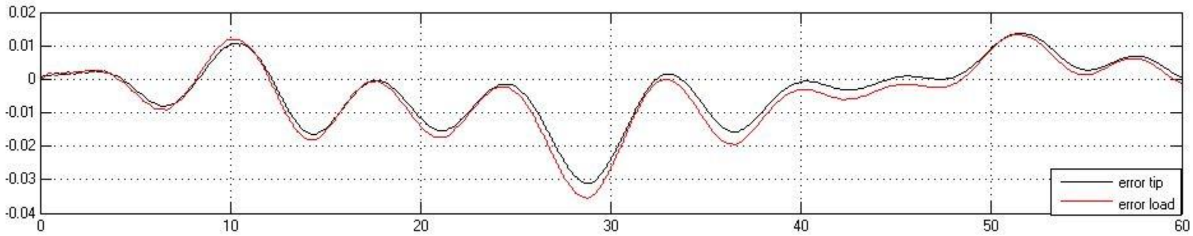

Figure 38 – Error of the crane tip and error of the load [m] versus time [s] for rotational system. Power consumption of the pump: 1.26 kWh.

The rotational system achieves a lower accuracy than the translational system. This issue was expected as the translational system is compensating for a 17.5 ton load plus the weight of 100 meters of cable, whereas the rotational system also has to deal with the entire inertia of the drum containing the remaining 2900 meters of cable. This was no issue for load case 1, because the drum was empty at that point. Resolving the remaining error relies on the feedback loop, because the feedforward controller does not account for it. However, the error is relatively small and therefore the proportional-derivative feedback action is not sufficient to overcome the problem. In the theoretical case that the inertia of the drum were neglected, the performance of the rotational system shows a similar response as the translational system in figure 37.

In terms of efficiency the larger drum works beneficial, because the drum contains 2900 meters of cable the effective drum diameter has increased. This means that the ratio between actuator velocity and cable velocity has increased, meaning that the motor has to rotate at a lower angular velocity to achieve the same reaction speed in the cable. The angular velocity of the motor is proportional to the required flow rate and therefore the power consumption of the pump.

The efficiency of the translational system remains the same as in load case 1. This was expected as the dimensions of the actuator do not change, so the actuator requires to same flow rate to compensate for the heave motion. This shows the problem with simple hydraulic systems. The actuators need to be designed for worst case scenarios and will therefore waste energy during relatively lesser load conditions. This problem was already briefly mentioned in the introduction of Chapter 3. Paragraph 7.3 will compare the performance and efficiency of more efficient translational and rotational systems.

7.3 Improved efficiencies

The translational systems often improve efficiencies by means of a nitrogen accumulator unit. The pressure from the accumulator can relief the system of inertia forces, such that the active cylinder can reduce substantially in size, requiring less fluid flow. The working principle of the accumulator unit has been described in Chapter 4. More advanced rotational actuation systems acquire a better efficiency by using motors with a variable stroke volume, for example with a swashplate motor. Both systems are schematically shown in figure 39.

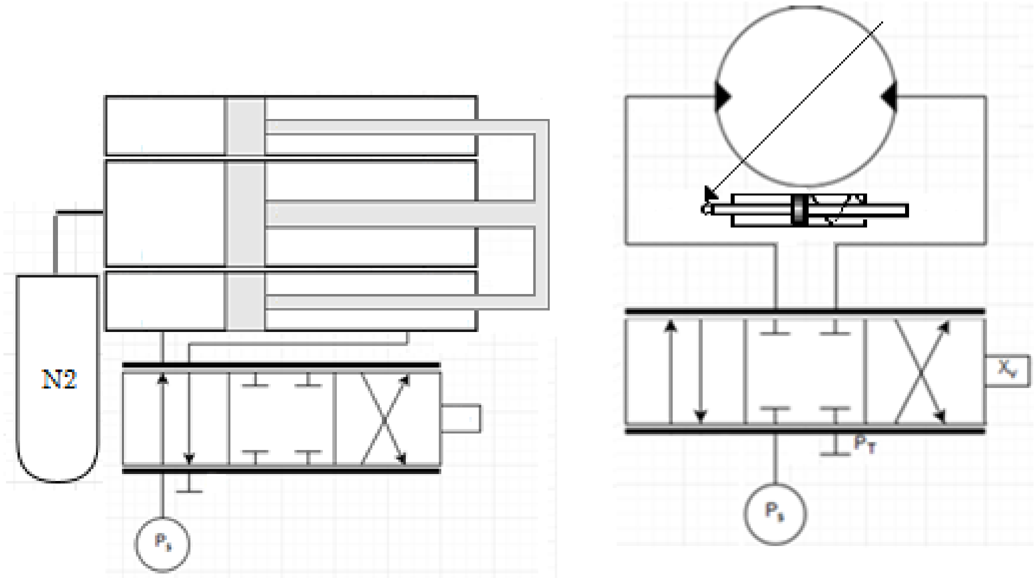

Figure 39 – More efficient translational and rotational heave compensation systems.

Hydraulic cylinder	Hydraulic motor
$D = 0.13\ \text{m}$	$D_m = 14\ \text{L/rad}$
$Q_{pump} = 650\ \text{L/min}$	$Q_{pump} = 1050\ \text{L/min}$
$P_{pump} = 275\ \text{kW}$	$P_{pump} = 450\ \text{kW}$

Table 7 – Actuator dimensions of the hydraulic cylinder and motor, respectively.

Table 7 shows the dimensions of the improved hydraulic systems, schematically shown in figure 39. The hydraulic cylinder can reduce in size, because the accumulator unit resolved the static forces in the system. The required cylinder diameter has reduced from 19cm to 11.5cm, which requires a maximum pump power of 275kW rather than 375kW. The hydraulic motor can also reduce in size, because the stroke volume is adjustable to the situation and there is no need to work with a load pressure with margin $p_L = 2/3\ p_s$. Only the maximum stroke volume is designed with this margin.

7.3.1 Load case 1

Operating depth: $L_c = 3000$ m.
Mass of the load: $m_l = 30$ ton.
Mass of the cable: $m_c = 12$ ton.

Figures 40 and 41 show the simulation results for the situation sketched in table 7 for load case 1. Both systems are designed for this load case, so not much difference in the responses is expected with respect to paragraph 7.2.1. The corresponding efficiencies should however be significantly better.

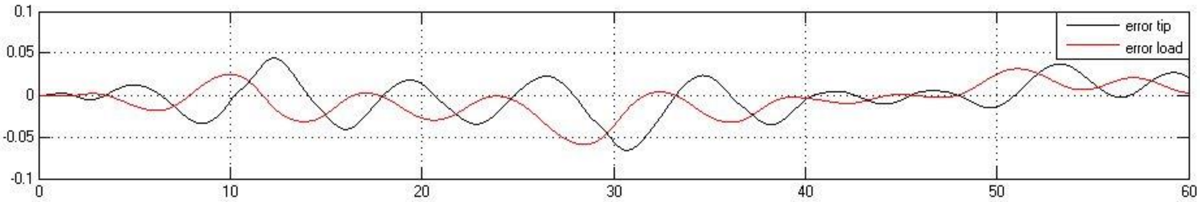

Figure 40 – Error of the crane tip and error of the load [m] versus time [s] for translational system. Power consumption of the pump: 0.60 kWh.

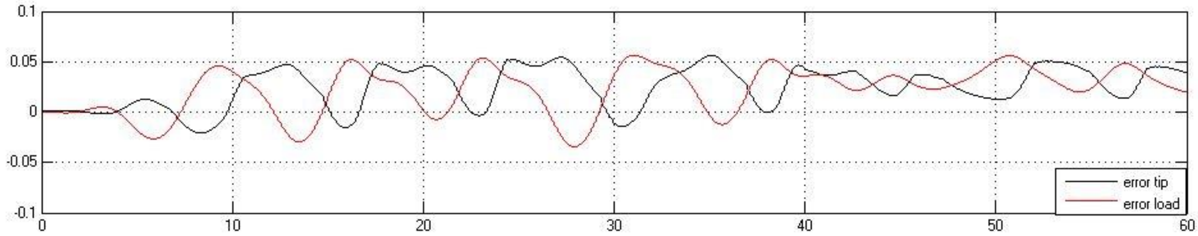

Figure 41 – Error of the crane tip and error of the load [m] versus time [s] for rotational system. Power consumption of the pump: 1.12 kWh.

The response is similar and of the same order as in figures 32 and 33 in paragraph 7.2.1. However, the pumps consume significantly less power with respect to their previous configurations. The efficiency of the translational system increased with 60%, whereas the efficiency of the rotational system increased with 23%. The fact that the increase in efficiency of the rotational system is relatively small, is because the motor stroke volume could only decrease slightly for this load case.

7.3.2 Load case 2

Operating depth: $L_c = 100$ m.
Mass of the load: $m_l = 30$ ton.
Mass of the cable: $m_c = 0.4$ ton.

Load case 2 considers the same systems at an operating depth of 100 meter. At this point the mass of the cable is negligible with respect to the mass of the load. Figures 42 and 43 show the performance of both systems under these operating conditions. For the rotational system the variable motor stroke volume reduced to 13 $\mathrm{L/rad}$.

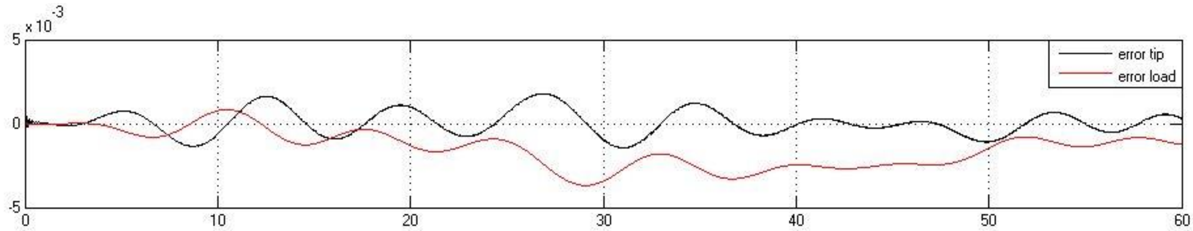

Figure 42 – Error of the crane tip and error of the load [m] versus time [s] for translational system. Power consumption of the pump: 0.60 kWh.

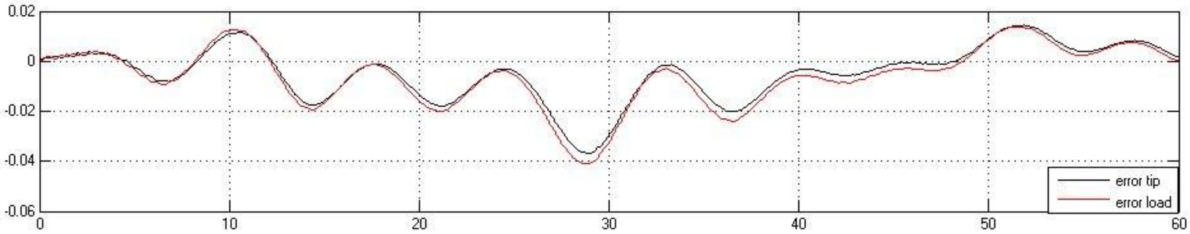

Figure 43 – Error of the crane tip and error of the load [m] versus time [s] for rotational system. Power consumption of the pump: 0.90 kWh.

Figures 42 and 43 show that also for load case 2 the same performance is achieved with a significantly higher efficiency. The translational system in figure 42 has even slightly improved accuracy with respect to figure 37, while improving the efficiency with 60%.

The rotational system in figure 44 achieved less accuracy with respect to figure 38. Reducing the motor stroke volume shows to have some impact on the accuracy as the system has more trouble compensating for the relatively high inertia of the drum. The magnitude of the error is however still relatively small and is therefore not problematic. The efficiency has improved with 29% with respect to the less efficient system in figure 38.

7.4 Summary

The translational and rotational systems were both compared for two configurations to analyse the differences with respect to performance and efficiency. In paragraph 7.2 the systems were designed for a given load case, similar to the test case in the TMS project. In paragraph 7.3 the systems were redesigned to improve efficiency. This gave more insight on performance versus efficiency for the different hydraulic actuation systems.

Translational systems show overall better performance. They tend to achieve a higher accuracy, because they only have to compensate for the mass of the load and cable, whereas the rotational systems also have to rotate the drum with a relatively high inertia. In terms of efficiency the translational system can be designed with a smaller active volume than the rotational system. Therefore it requires less fluid flow to compensate for the heave motion. Efficiency can be further improved by implementing a nitrogen accumulator unit. Simulations have shown that this reduces the power consumption of the translational system with 60%. The rotational system can improve efficiency by using a variable displacement motor. This makes it possible to reduce the motor stroke volume when a smaller load is applied. This can save up to 29% of the power consumed by the pump.

Considering the rotational system with respect to the test case of the TMS crane in Chapter 6 the accuracy has been increased with almost 75% by using velocity feedforward and tension control. One should keep in mind that this is a theoretical value, achieved by using perfect sensors that do not account for delay, noise and limited accuracy. Also the velocity feedforward is only as accurate as the description of the plant. In practice the improvements will be lower, but the simulations offer a good insight on the possibilities regarding feedforward and tension control.

8 Conclusion and discussion

8.1 Conclusion

The focus in this report lay on the performance of the hydraulic components in the heave compensation systems for offshore cranes. Translational and rotational actuation systems are modelled, simulated and compared. Both systems are modelled in exactly the same fashion in order to make a fair comparison. Both systems are subjected to a heave motion that originates from a wave model using superposition of different sine frequencies and amplitudes to generate a wave pattern. The heave motion of the vessel is assumed to be measured at a motion reference unit at the base of the crane. The respective heave motion of the crane tip is derived using transformation matrices, the crane is assumed rigid in this process.

Simulations show that the translational system is able to achieve the highest accuracy and efficiency. Extended with a passive cylinder connected to a nitrogen accumulator, it has the ability to counter static forces like the inertia of the load. This technique is often used in practice and is therefore also taken into account. Translational systems with accumulator can be applied on a much wider range of operating conditions, with high efficiency and without becoming too large.

The rotational system uses only the components that are already present in a standard configuration for raising and lowering a load. Also it does not require extra guiding sheaves for the cable as in the translational system, which greatly increases the cable lifetime. The translational system is unable to compensate for heave motions beyond the cylinder stroke, which often results in over-dimensioned systems that require relatively large operating space, which is scarce aboard a vessel. These arguments cannot be measured in a simulation and are therefore left open for discussion. Simulations have shown that the rotational system has relatively more trouble at lower operating depth, caused by the inertia of the remaining cable on the drum. Translational systems have no issues here as they are not influenced by the drum.

Velocity feedforward is applied which significantly improves the accuracy of both actuation systems. Stability of the system has been improved using tension feedback and especially the position error of the load has been greatly reduced. Without the tension feedback the load attached to a cable shows increasingly large oscillatory motion of the load for greater operating depths as the cable stiffness decreases. In frequency regions close to the natural frequency of the cable this oscillatory behaviour caused resonance in the cable and made the system unstable. This problem no longer occurs when using tension feedback.

8.2 Discussion

Translational and rotational heave compensation systems have been analysed on performance and efficiency with respect to a test case within the TMS project. Improvements with regard to accuracy are achieved by improving the controller. These are all theoretical values that offer a good insight on the possibilities regarding feedforward and tension control. It is suggested to test these control strategies in an experimental setup, to compare the simulation results with practical test results.

In terms of efficiencies both systems have been compared to more efficient designs that are currently encountered in practice. Simulations have shown to what extend these designs improve efficiencies. However, there are several more methods for saving energy that are not taken into account. Therefore it is suggested to do more research on efficient hydraulic methods, like using a variable pump or redirecting fluid between cylinder chambers, etcetera. These methods can then be modelled and simulated to give an indication on the effectiveness of each method.

In this report all simulations are performed at a given operating depth, which eliminates various interesting subjects and scenarios. For one the knuckle boom crane is assumed rigid and stationary. It would be interesting to see the effects of the dynamic behaviour of the crane on the position error of the crane tip. For example the deflection of the crane tip by bending may have significant influence on the overall accuracy of the system. Other subjects that come to mind are a complete simulation of lowering the load including the point of water entry. This can give insight on whether the heave compensation system is able to smoothen this process. Also a completely controllable knuckle boom crane can be taken into account, which offers the possibility of a full simulation from vessel deck to sea bed. Suggestions for crane control were already given in Chapter 2.

Bibliography

1. Journée, J.M.J. and Massie, W.W. (2001). Offshore Hydromechanics (1st edition). Delft University of Technology.

2. Fossen, T. I. and Perez T. (2004). Marine Systems Simulator (MSS). <http://www.marinecontrol.org>.

3. Albers, P. (2010). Motion Control in Offshore and Dredging. Delft University of Technology.

4. Gregov, G. and Siminiati, D. (2010). Computer simulation of a laboratory hydraulic system with matlab-simulink.

5. Sverdrup-Thygeson, J. (2007). Modeling and simulation of an active hydraulic heave compensation system for offshore cranes. Norwegian University of Science and Technology Department of Engineering Cybernetics.

6. Choux, M. and Hovland, G. (2008). Design of a hydraulic servo system for robotic manipulation. University of Agder.

7. Rydberg, K-E. (2008). Hydraulic servo systems – Theory and applications. Linköping University.

8. Kroneld, P. Liedes T. Nevala K. Marjanen Y. (2006). Modelling a selective hydropneumatic suspension element. University of Oulu.

9. Tomasgard, G. (2008). Real-time simulation of offshore light lift operations. Norwegian University of Science and Technology Department of Engineering Cybernetics.

10. Larsen J. M. (2010). Validation study of real gas models - Applied on a wide range of temperatures and pressures. Aalborg University.

Appendix I – Simulink models

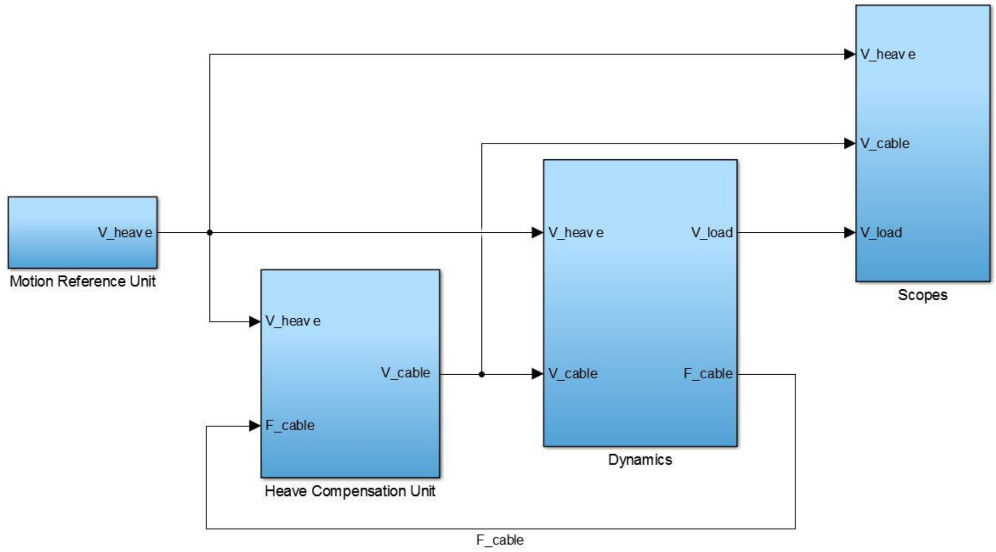

Figure 44 – Simulink Assembly model.

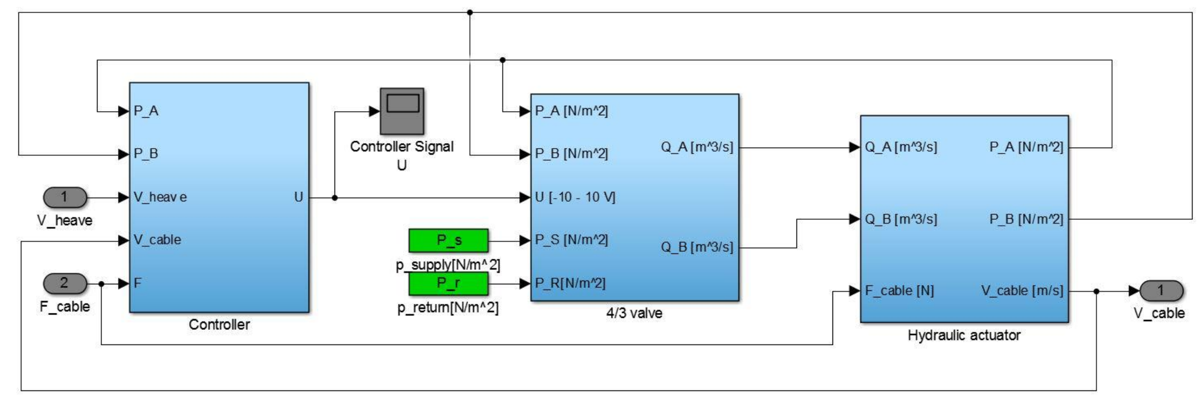

Figure 45 – Simulink model heave compensation system.

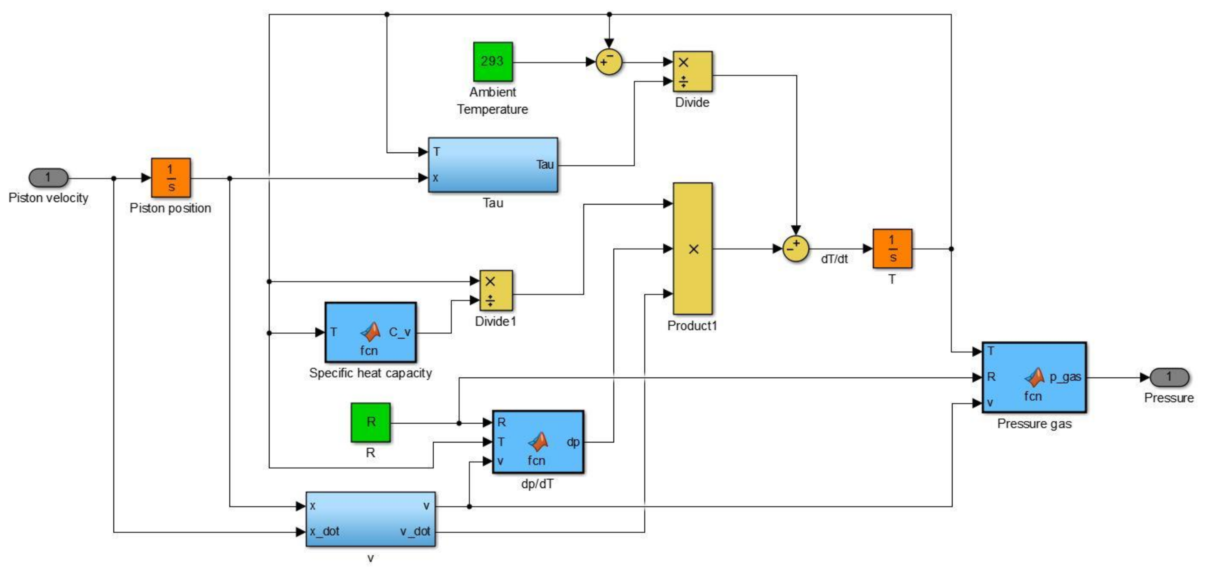

Figure 46 – Simulink model nitrogen accumulator.